

720
2018

Berichte

zur Polar- und Meeresforschung

Reports on Polar and Marine Research

The Expedition PS98 of the Research Vessel POLARSTERN to the Atlantic Ocean in 2016

Edited by

Bernhard Pospichal

with contributions of the participants

Die Berichte zur Polar- und Meeresforschung werden vom Alfred-Wegener-Institut, Helmholtz-Zentrum für Polar- und Meeresforschung (AWI) in Bremerhaven, Deutschland, in Fortsetzung der vormaligen Berichte zur Polarforschung herausgegeben. Sie erscheinen in unregelmäßiger Abfolge.

Die Berichte zur Polar- und Meeresforschung enthalten Darstellungen und Ergebnisse der vom AWI selbst oder mit seiner Unterstützung durchgeführten Forschungsarbeiten in den Polargebieten und in den Meeren.

Die Publikationen umfassen Expeditionsberichte der vom AWI betriebenen Schiffe, Flugzeuge und Stationen, Forschungsergebnisse (inkl. Dissertationen) des Instituts und des Archivs für deutsche Polarforschung, sowie Abstracts und Proceedings von nationalen und internationalen Tagungen und Workshops des AWI.

Die Beiträge geben nicht notwendigerweise die Auffassung des AWI wider.

Herausgeber

Dr. Horst Bornemann

Redaktionelle Bearbeitung und Layout

Birgit Reimann

Alfred-Wegener-Institut
Helmholtz-Zentrum für Polar- und Meeresforschung
Am Handelshafen 12
27570 Bremerhaven
Germany

www.awi.de

www.reports.awi.de

Der Erstautor bzw. herausgebende Autor eines Bandes der Berichte zur Polar- und Meeresforschung versichert, dass er über alle Rechte am Werk verfügt und überträgt sämtliche Rechte auch im Namen seiner Koautoren an das AWI. Ein einfaches Nutzungsrecht verbleibt, wenn nicht anders angegeben, beim Autor (bei den Autoren). Das AWI beansprucht die Publikation der eingereichten Manuskripte über sein Repositorium ePIC (electronic Publication Information Center, s. Innenseite am Rückdeckel) mit optionalem print-on-demand.

The Reports on Polar and Marine Research are issued by the Alfred Wegener Institute, Helmholtz Centre for Polar and Marine Research (AWI) in Bremerhaven, Germany, succeeding the former Reports on Polar Research. They are published at irregular intervals.

The Reports on Polar and Marine Research contain presentations and results of research activities in polar regions and in the seas either carried out by the AWI or with its support.

Publications comprise expedition reports of the ships, aircrafts, and stations operated by the AWI, research results (incl. dissertations) of the Institute and the Archiv für deutsche Polarforschung, as well as abstracts and proceedings of national and international conferences and workshops of the AWI.

The papers contained in the Reports do not necessarily reflect the opinion of the AWI.

Editor

Dr. Horst Bornemann

Editorial editing and layout

Birgit Reimann

Alfred-Wegener-Institut
Helmholtz-Zentrum für Polar- und Meeresforschung
Am Handelshafen 12
27570 Bremerhaven
Germany

www.awi.de

www.reports.awi.de

The first or editing author of an issue of Reports on Polar and Marine Research ensures that he possesses all rights of the opus, and transfers all rights to the AWI, including those associated with the co-authors. The non-exclusive right of use (einfaches Nutzungsrecht) remains with the author unless stated otherwise. The AWI reserves the right to publish the submitted articles in its repository ePIC (electronic Publication Information Center, see inside page of verso) with the option to "print-on-demand".

*Titel: Kurzer Regenschauer, charakteristisch für feuchte Luftmassen über warmen subtropischen Ozeanen.
Aufnahmeort: Südatlantik östlich von Brasilien (25°S, 38°W) am 19.04.2016 (Foto: B. Pospichal).*

Cover: Short rain shower, characteristic of moist air masses over warm subtropical seas. Picture taken in the South Atlantic Ocean east of Brazil (25°S, 38°W) on April 19th, 2016 (Photo: B. Pospichal).

The Expedition PS98 of the Research Vessel POLARSTERN to the Atlantic Ocean in 2016

**Edited by
Bernhard Pospichal
with contributions of the participants**

Please cite or link this publication using the identifiers

**<http://hdl.handle.net/10013/epic.559e1f61-c6f4-4f03-8725-f553b9204adc> and
https://doi.org/10.2312/BzPM_0720_2018**

ISSN 1866-3192

PS98

(ANT-XXXI/4)

10 April – 11 May 2016

Punta Arenas – Las Palmas – Bremerhaven

**Chief scientist
Bernhard Pospichal**

**Coordinator
Rainer Knust**

Contents

1.	Zusammenfassung und Fahrtverlauf	2
2.	Weather Conditions	5
3.	Autonomous Measurement Platforms for Energy and Material Exchange between Ocean and Atmosphere (OCEANET): Atmosphere	8
3.1	Raman Lidar observations	8
3.2	Microwave radiometer observations	11
3.3	Shadowband radiometer observations for cloud and aerosol property retrieval	12
3.4	Infrared camera measurements for temperature profiling	14
4.	Documenting Aerosol and Cloud Parameters across Different Oceanic Climate Regions	15
4.1	Aerosol extinction measurements	15
4.2	Cloud observations	18
4.3	Other activities	24
5.	Animal Transport for Studies on Temperature and Hypoxia Tolerance of Various Life Stages of Lithodid Crabs	25
6.	Echosounding Training Cruise (Polmar-Train 2016)	33
	Appendix	
A.1	Teilnehmende Institute / Participating Institutions	39
A.2	Fahrtteilnehmer / Cruise Participants	41
A.3	Schiffsbesatzung / Ship's Crew	43
A.4	Stationsliste / Station List	46

1. ZUSAMMENFASSUNG UND FAHRTVERLAUF

Bernhard Pospichal

Universität Leipzig

Der Fahrtabschnitt PS98 war der letzte der Antarktissaison 2015/16 von *Polarstern* und begann planmäßig am 10. April 2016 in Punta Arenas, wo 14 Wissenschaftler an Bord gingen. Die Fahrtroute (Abb. 1.1) führte nach dem Verlassen der Magellanstraße auf direktem Weg nach Las Palmas. Der Äquator wurde in der Nacht vom 25. zum 26. April 2016 überquert.

Schwerpunkt des ersten Teils der Fahrt waren atmosphärische Beobachtungen. Dabei wurden, wie bereits auf mehreren vergangenen Atlantiküberfahrten im Rahmen des OCEANET-Projekts, Messungen zu Aerosol, Wolken und Wasserdampf entlang der Fahrtroute durchgeführt. Dazu wurden unter anderem ein Ramanlidar, ein Mikrowellenradiometer, ein Sonnenphotometer sowie mehrere Messgeräte zur atmosphärischen Strahlung kontinuierlich betrieben. Himmelskameras im sichtbaren sowie im infraroten Wellenlängenbereich gaben Auskunft über die räumliche Verteilung von Wolken. Darüber hinaus wurde erstmals auch eine scannende Infrarot-Wolkenkamera eingesetzt, um damit Wolkenseiten zu beobachten.

Eine Besonderheit der Fahrt waren kurzfristige Anpassungen der Route an die Überflüge des sogenannten A-Train, einer Satellitenkonstellation, die insbesondere ein weltraumgestütztes Aerosol-Lidar (CALIOP) und Wolkenradar (CLOUDSAT) beinhaltet. Hierdurch ergab sich die einzigartige Gelegenheit, Wolken- und Aerosolprofile simultan aus Satelliten- und Bodenperspektive über dem Ozean zu erhalten. Leider war es bei den meisten Überflügen bewölkt, sodass die Aerosolprofile nur begrenzt verglichen werden konnten.

Unterwegs wurden auch fünf autonome Floats für Temperatur- und Salzgehaltsmessungen im Rahmen des internationalen ARGO-Programms ausgesetzt.

Las Palmas wurde am 03. Mai erreicht, wo weitere 25 Fahrtteilnehmer an Bord kamen, die Teil eines Ausbildungskurses zur seismischen Methoden waren. 20 Doktoranden und Masterstudenten hatten ein intensives sechstägiges Programm, bei dem verschiedene Verfahren zur Sedimentakustik angewandt wurden.

Der letzte Fahrtabschnitt endete am 11. Mai 2016. *Polarstern* erreichte mit dem Abendhochwasser die Nordschleuse in Bremerhaven, um dann gegen 19 Uhr am Kai des Heimathafens festzumachen.

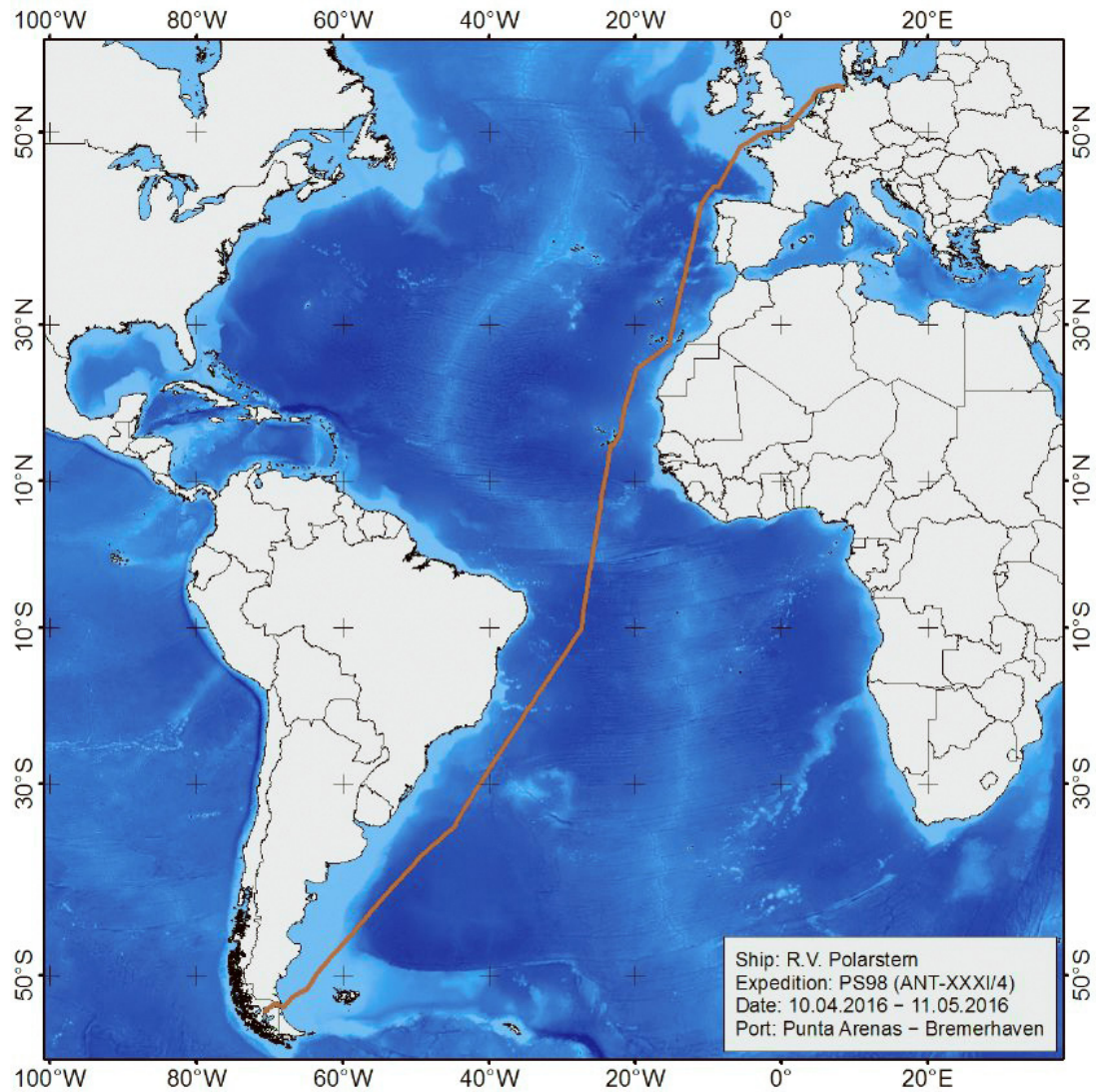


Abb. 1.1: Kurskarte der Polarstern Expedition PS98.
Siehe <https://doi.pangaea.de/10.1594/PANGAEA.863107> für eine Darstellung des master tracks in Verbindung mit der Stationsliste für PS98.

Fig. 1.1: Cruise track of RV Polarstern during the expedition PS98.
See <https://doi.pangaea.de/10.1594/PANGAEA.863107> to display the master track in conjunction with the list of stations for PS98.

SUMMARY AND ITINERARY

PS98 was the last expedition of the Antarctic season 2015/16 of *Polarstern* and started in Punta Arenas on 10 April 2016 as scheduled. 14 scientists took part in this section. After leaving the Strait of Magellan, the route of *Polarstern* (Fig. 1.1) led directly towards Las Palmas. On the way the equator was crossed during the night from 25 to 26 April.

The cruise leg until Las Palmas was dominated by Atmospheric observations in the frame of the OCEANET project. Like at several previous crossings of the Atlantic Ocean, measurements of aerosol, clouds and water vapor have been performed during the cruise. For this purpose, a Raman lidar, a microwave radiometer, a sun photometer, as well as several instruments for measuring different components of the atmospheric radiation were continuously operated. Sky cameras in visible and infrared wavelength observed the spatial variability of clouds. In addition, a scanning infrared cloud camera was operated to perform cloud side observations.

On this cruise short-term adaptations of the route were performed in order to directly meet satellite overpasses of the A-train constellation, which consists of several satellites, most notably the spaceborne aerosol lidar (CALIOP) as well as a cloud radar (CLOUDSAT). With these observations, a unique possibility was found to get simultaneous cloud and aerosol profiles from satellite and ground perspective over the Ocean. Unfortunately, most of the overpasses were cloud covered, and no aerosol profiles could be derived.

On the way, five autonomous floats for temperature and salinity observations were deployed in the frame of the international ARGO programme.

Las Palmas was reached on 3 May where 25 new cruise participants came on board. They were part of a training course for seismic methods. 20 PhD and Master students had an intense programme on the following six days applying different methods of sediment acoustics.

The last cruise leg ended on 11 May 2016. *Polarstern* arrived at the Northern locks in Bremerhaven with the evening high tide and docked at the quay of its home port at around 7 pm.

2. WEATHER CONDITIONS

Hartmut Sonnabend

Deutscher Wetterdienst

Polarstern left the harbour of Punta Arenas for the cruise leg PS98 on 10 April 2016 at 18:00 local time. Located between strong cyclonic activity over the sea areas around the Antarctic Peninsula and a belt of high pressure extending from the Southeast Pacific across Patagonia towards the sea areas east of Argentina, the wind quickly freshened up to force 6 – 7 Bft. from northwest to west. These conditions persisted until the afternoon of 11 April, when a high pressure ridge swinging across the cruise line caused a decrease to Bft. 4 during the evening and night. Along the south-western flank of the above mentioned anticyclone which meanwhile had reached the area south of the mouth of Rio de la Plata and a flat trough forming along the eastern part of Patagonia, the wind shifted to northwest again and soon breezed up to strength 6 - 7 with gusts up to Bft. 8 during the afternoon of the following day. This constellation with strong to stormy winds from the northwest was peaking in a wind speed between 30 – 35 knots and corresponding wave heights of around 3 m during the morning of 13 April. Until the evening of this day the wind decreased only slowly. In the meantime, a flat low coming from Uruguay tracked south-eastward north of the cruise line of *Polarstern* during the following night, while intensifying to a small gale centre. Its swell, having been generated by the storm over the sea areas east of its centre, passed the position of *Polarstern* around noon of 14 April with maximum wave heights of around 3 m. By same time the wind breezed up to Bft. 6 – 7 from west between the rear of the withdrawing gale centre and a following high pressure ridge. Under the influence of this ridge swinging across the cruise line, the wind calmed down during the next night. Embedded between a large low pressure trough extending from Tierra del Fuego across Argentina towards Paraguay and Bolivia and the southwestern flank of the South Atlantic Subtropical High, the wind shifted to northwest and northnorthwest again and increased to yet another strong wind event. Meanwhile the cold front of a low pressure trough east of Tierra del Fuego became nearly stationary over the Rio de la Plata area and converted into an air mass boundary, separating warm and moist air in the north from cooler air of subpolar origin in the south. This development resulted in a brisk shower- and thunderstorm-activity on the warm side over Uruguay and the mouth of Rio de la Plata, spreading east-southeastward across the cruise line of *Polarstern*. During the night to 16 April, thunderstorms associated with heavy rain and gusts up to Bft. 9 were observed. These conditions with predominantly convective rain and some isolated embedded thunderstorms lasted until forenoon of this day. After having left behind the area of the convergence with its bad weather, the strong north-westerly wind decreased gradually during the night to 17 April, levelling to a moderate breeze from northwest to west.

The further course of *Polarstern* led along the western, north-western and northern flank of the South Atlantic Subtropical High, located with its centre between latitude 25° and 30° south, initiating the transition to a moderate trade wind circulation from northerly to north-easterly directions. Some light rain showers were recorded during morning and forenoon of 19 and 21 April. Crossing the sea areas between the northern flank of the Subtropical High in the south and the Equatorial Trough in the north, the wind shifted to easterly and finally south-easterly directions. Apart from a short break during the second part of 22 April, the trade wind blew as a fresh to strong breeze with force 5 – 6 Bft. until afternoon of 25 April. One more rain

shower was observed during the night to this day. Encountering the Equatorial Trough, the wind started to decrease to a moderate south-easterly breeze. During 26 April, we entered the region of the Inter Tropical Convergence Zone (ITCZ) with a light breeze until evening. In the environment of the cruise line the ITCZ presented as a relatively well organized band of predominantly cumulonimbus clouds extending between 3.5°N and 5.5°N. One of these deep convection cells produced a heavy rain shower in the evening of 26 April. During the following night however only distant lightning was observed temporarily.

The crossing of the ITCZ marked the transition into the trade wind system of the Northeast Atlantic. Along the southeast flank of a weak high centred southwest of the Canary Islands a moderate breeze of force 4 – 5 Bft. from north to northeast set in during the morning of 27 April. The following days brought only little change to these conditions with predominantly moderate north-easterly winds. Underneath a strong trade wind inversion, dense fields of stratocumulus clouds formed up overnight frequently, making place for the sun not before noon or afternoon. Additionally, a band of high and medium high clouds drifting across the cruise line of *Polarstern* hampered measurements especially on 30 April. Between a strengthening subtropical high pressure ridge extending from the sea areas west of the Canary Islands towards the regions northwest of the Cape Verde Islands and the seasonal trough over the western and north-western Saharan desert, the trade wind accelerated during evening of 30 April, peaking force 6 – 7 Bft. during morning and noon of 1 May. A rough sea of about 2.5 m from ahead was induced. The conditions improved when the axis of the high pressure ridge moved further westward causing a weakening of the air pressure gradient during the second part of this day. Apart from coastal effects in the vicinity of Gran Canaria, when the northerly to north-northwesterly wind accelerated to force 6 with gusts up to 7 – 8 for a short time, the final approach to Las Palmas proceeded at a moderate trade wind from ahead. *Polarstern* entered the port of Las Palmas on 3 May at 14:00 local time.

On the same day at 22:30 *Polarstern* left the harbour of Las Palmas for its final cruise leg to Bremerhaven at a light to moderate north-westerly breeze. Meanwhile a shallow trough coming from the Atlantic coast of Morocco had reached the sea areas east of Madeira putting an end to the previous trade wind circulation. During the next two days this flat trough spread across the Iberian Peninsula towards the Bay of Biscay. The moderate to fresh wind shifted southwest for a while during 4 May, to turn into a light northerly breeze next day. On the back side of the north-northeastward tracking trough the wind freshened up to Bft. 6 from northwest during morning and forenoon of 6 May. In the early morning of 7 May, *Polarstern* encountered the circulation area of a large storm depression centred near 40° North/18°West with a minimum air pressure of 985 hPa. Associated with continuous rainfall the wind breezed up to force 7 and occasionally 8 Bft. from south to southeast. Wave heights reached a maximum of around 3 meters for a while. After having passed Cape Finisterre and entered the Bay of Biscay wind and wave conditions calmed down soon. The following transit through the Biscay brought only moderate to fresh winds from east-southeast to southeast. On 9 May, when passing Brittany and entering the English Channel, fresh to strong easterly to east-southeasterly winds dominated in the vicinity of the north-eastward swinging cold front, belonging to the gale centre west of Biscay. During early morning hours of 10 May, *Polarstern* encountered large fog patches, triggered by warm and very moist air above the relative cold water. Light to moderate rainfall caused additional reduce of visibility by same time. Advection of drier air from the nearby land allowed a temporary improvement of the visibility just during our passage through the Strait of Dover. Continuing our course towards the south-western North Sea visibility changed to poor with some flat fog patches soon for the rest of this day. Fresh to strong easterly to east-northeasterly winds predominated during our final cruise leg towards the Weser Pilot and into the mouth of Weser River. *Polarstern* entered the harbour of Bremerhaven in the evening of 11 May 2016.

For further statistics see attached graphs (Fig. 2.1 – Fig. 2.3).

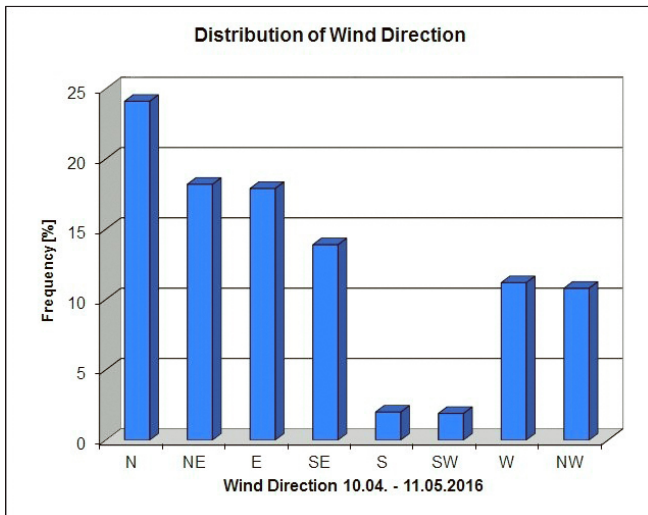


Fig. 2.1: Distribution of wind direction

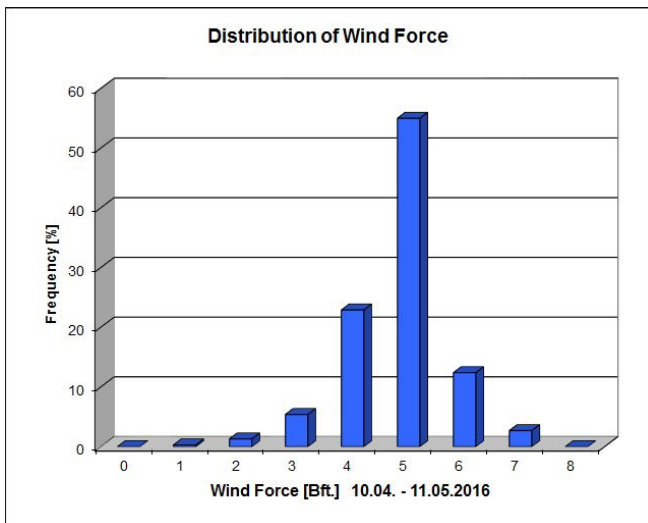


Fig. 2.2: Distribution of wind force

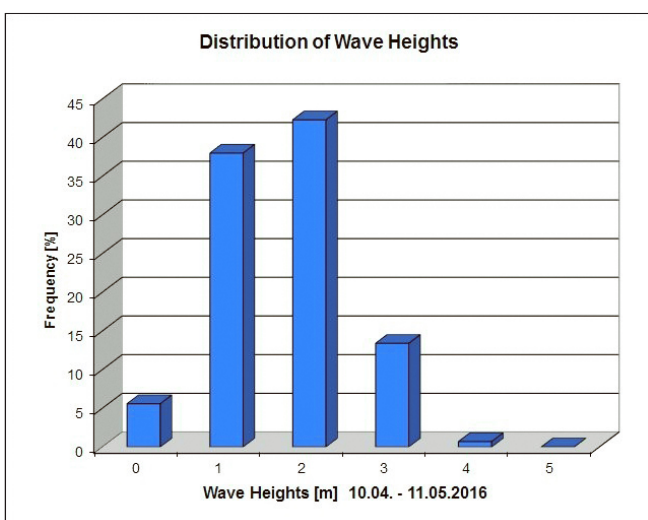


Fig. 2.3: Distribution of wave heights

3. AUTONOMOUS MEASUREMENT PLATFORMS FOR ENERGY AND MATERIAL EXCHANGE BETWEEN OCEAN AND ATMOSPHERE (OCEANET): ATMOSPHERE

Bernhard Pospichal¹, Stephanie Bohlmann²,
Tobias Doktorowski¹, Tobias Kuchler^{1,2}, Martin
Radenz², Johannes Stapf¹
not on board: Andreas Macke², Ronny
Engelmann²

¹LIM
²TROPOS Leipzig

AWI_PS98_00

Introduction

The net radiation budget at the surface is an important regulator in the climate system of the Earth. Next to well-known greenhouse gas effects it is mainly influenced by the complex spatial distribution of aerosols and clouds (liquid and ice water clouds) in the atmosphere. The complex interaction between aerosol particles and cloud particles still causes many uncertainties in climate models. While aerosol can directly scatter and absorb light depending on their type and chemical composition they also act as cloud condensation nuclei (CCN) and ice nuclei (IN).

To collect data for a better understanding of aerosols and clouds, scientists from the Leipzig Institute for Meteorology (LIM) at the University of Leipzig and the Leibniz Institute for Tropospheric Research (TROPOS) (Jun.-Prof. B. Pospichal, S. Bohlmann, T. Doktorowski, T. Kuchler, M. Radenz, J. Stapf) were aboard the PS98 transect. Several remote sensing and *in-situ* instruments were on board. The OCEANET container was installed at the bridge top ("Peildeck" on starboard). The measurements are used to increase the statistical dataset over the Atlantic where observations are extremely sparse.

As a further aspect, the route was chosen to obtain optimal matchups with *CALIPSO*, satellite of the A-Train constellation. The resulting datasets will offer the unique opportunity to compare vertically resolved profiles of clouds and aerosols from the satellite and ground-based perspective over the ocean.

3.1 Raman Lidar observations

Stephanie Bohlmann, Martin Radenz

TROPOS Leipzig

Objectives

One major instrument is the multiwavelength Raman lidar (type: Polly-XT) which measures profiles of the backscatter coefficient at three wavelengths, of the extinction coefficient and of the depolarisation at two wavelengths as well as of the water-vapour mixing ratio.

The portable lidar Polly performed 24/7 measurements aboard *Polarstern*, whenever the weather conditions were appropriate. This 3+2+2+1 Raman/polarization and water-vapour lidar provides highly temporal resolved information about the vertical distribution of aerosols

and water vapour. Aerosol particle optical properties in terms of the particle backscatter and extinction coefficient can be determined directly and serve as input for height-resolved inversion methods to estimate the main microphysical properties (e.g. size distribution) at any measured height. Thus, lofted free-tropospheric aerosol layers can be characterized separately from the marine boundary layer. Typical known free-tropospheric aerosols are anthropogenic emissions from North America, dust from the Saharan region or smoke from biomass burning in Central Africa. These aerosols can be lifted up above land and are transported over the Atlantic Ocean for several days. During this transport, the aerosols influence the radiation budget of the Earth. Thus, the height-resolved information as derived from lidar is a crucial input for radiative transfer calculations to determine the direct aerosol radiative effect more precisely. In addition, the height-resolved measurements offer the opportunity to determine the extent of simultaneous occurring clouds, as well as the clouds state of phase to investigate aerosol-cloud interactions and to determine the indirect aerosol radiative effect, which shows the highest uncertainties in climate research.

Two All Sky Cameras are also mounted on the roof taking pictures every 20 sec. Also the DWD meteorological station measures standard parameters such as temperature, pressure, humidity, and solar and infrared radiation on a 1-s time basis.

Work at sea

The OCEANET container includes several instruments for the remote characterisation of aerosols and clouds. Measurements were taken en-route and are not depending on any station work. It was deployed on the bridge top. The instrument container was set up on 10 April in Punta Arenas. The lidar was taken into operation during the night to 11 April. After overlap adjustment, routine measurements started on 13 April.

Regrettably, the 1064 nm detector had a technical failure that could not be fixed during the cruise. Therefore, no backscatter measurements at this wavelength are available.

Regular maintenance procedures included daily cleaning on the radiation sensors and the All Sky Camera dome. The lidar window was also cleaned on a regular basis depending on obvious sea-spray or other contamination. Starting from 25 April to 4 May the lidar was turned off for 2-3 h during noon because of high sun elevation. Direct sunlight must be prevented from entering the telescope.

Preliminary (expected) results

After starting regular measurements in the night to 13 April the weather was dominated by clouds. Only a few cloud gaps could be observed. Fig. 3.1 presents the lidar quicklooks of the range-corrected signal at 532 nm and the volume depolarization ratio at 532 nm wavelength of the whole measurement period. On 14 April depolarizing layers could be observed. According to the HYSPLIT backward trajectories the air mass originated from the Patagonian Desert. Observations on 16 and 17 April were dominated by low clouds and rain.

On 22 April the lidar was able to detect a lofted plume of Saharan dust from 1.5 km to 3.5 km height above the marine boundary layer.

Crossing the Intertropical Convergence Zone (at around 5°N) on the 27 and 28 April, thunderstorms, rain showers and clouds with low base heights were predominant. After leaving this region the lidar could again observe Saharan dust. The dust bottom height of the dust layer decreased down to around 600 m on 30 April. In the afternoon of 1 May *Polarstern* left the dust region.

3.1 Raman Lidar observations

When reaching the port of Las Palmas on 3 May the lidar was turned off for several hours and turned on again after leaving the Canaries. Towards the end of the transect aerosol conditions were more and more influenced by anthropogenic sources. Preliminary analysis indicates a complex mixture of marine aerosols, dust and anthropogenic pollution. From 6 May mostly overcast sky with only small cloud gaps was predominant.

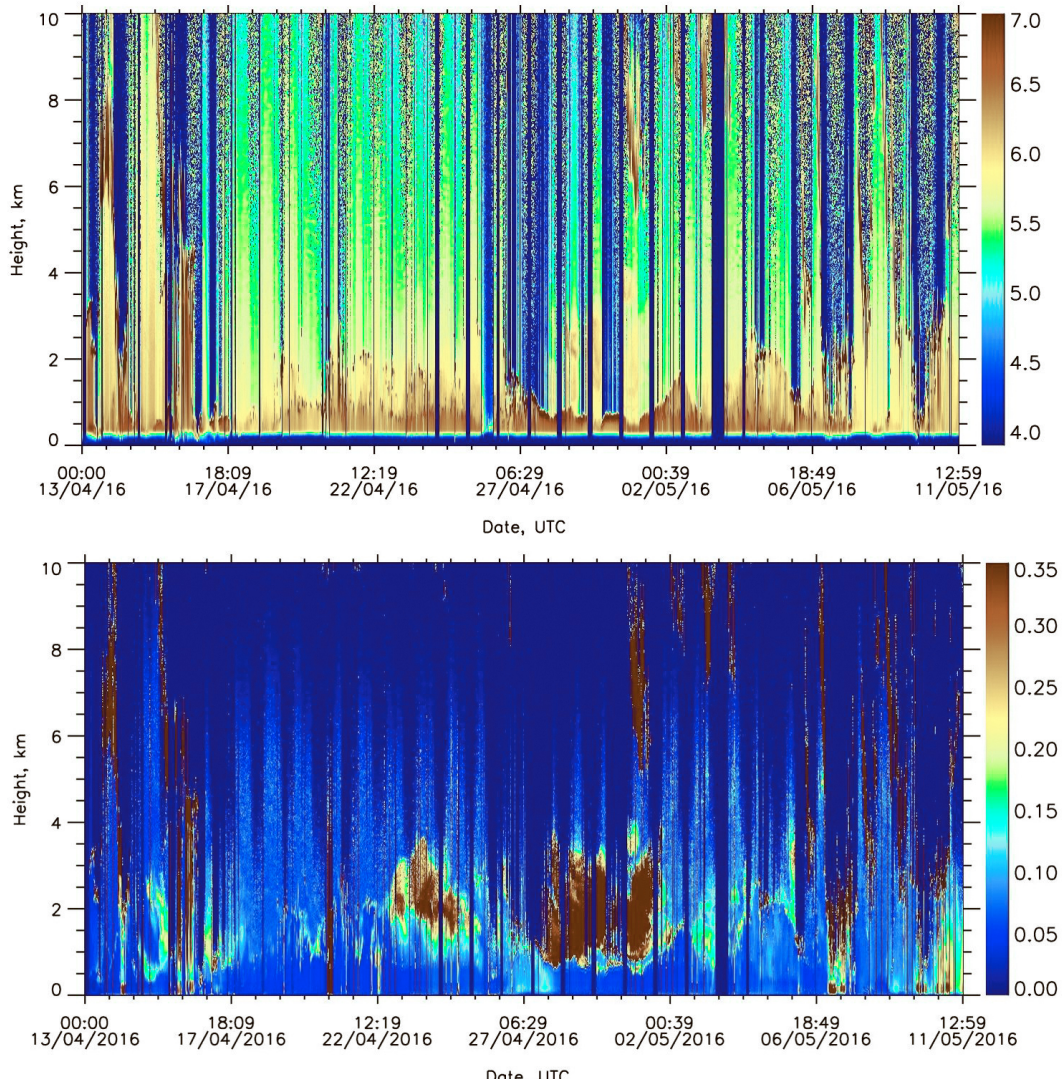


Fig. 3.1: Range-corrected lidar signal at 532 nm wavelength (top) and volume depolarization ratio at 532 nm wavelength (bottom)

See end of chapter 3.4 for data management.

3.2 Microwave radiometer observations

Bernhard Pospichal¹, Tobias Doktorowski²

¹LIM

²TROPOS Leipzig

Objectives

Observations of ship-based zenith looking passive microwave radiometer are a useful tool for determining the thermodynamic profile of the atmosphere. These instruments measure the thermal emission of atmospheric constituents in the microwave range in seven frequencies along the 22 GHz water vapor line and seven frequencies in the 60 GHz oxygen complex. From these measurements, temperature and humidity profiles as well as vertically integrated water vapor (IWV) and cloud liquid water (LWP) can be derived.

PS98 was already the 14th transatlantic cruise with this instrument on board of *Polarstern*, the first one ANT-XXIII/10 (PS69) in 2007. With this long dataset it will soon become possible to determine the inter-annual variability of the atmospheric conditions over the tropical and sub-tropical Atlantic Ocean.

Work at sea

During PS98, the HATPRO microwave radiometer was installed on top of the OCEANET container which was located on the starboard side of the upper deck. Before departure, a calibration with liquid nitrogen was performed when *Polarstern* was still at the pier in Punta Arenas, in order to guarantee stable and reliable measurements. The work at sea consisted of regular cleaning of the instrument housing as well as data quality control. During the cruise the instrument was operated continuously. The standard operation mode is zenith looking with a temporal resolution of 1 second. During PS98, improved temperature profiles were measured, by performing scans at different elevation angles every 15 minutes. Previously, it was thought that the accuracy of these scans might be influenced by lateral ship movements, although we could verify that the derived temperature profile did benefit greatly from the addition of elevation scans.

Preliminary (expected) results

Fig. 3.2 presents the time series of continuous temperature profiles along the route. Whereas the temperature usually decreases with height, the strong trade wind inversion around 30 April is clearly visible with higher temperatures at 1 km compared to the values at sea level. The low pressure system on 7 May west of Portugal caused a significant intrusion of cold air masses in upper levels. Furthermore, cross-sections of relative humidity, IWV and LWP (not shown) were produced. With now 10 years of observation, these data will be analysed together with those from previous cruises for some statistical analysis.

The measurements of temperature profiles in the marine boundary layer can give valuable information on the stability conditions over the Ocean. With the addition of elevation scans, this question can now be answered in more detail. In the master's thesis of Tobias Doktorowski, this effect was quantified using data from PS98. Compared to radiosondes, the bias is largely reduced and the root mean square error of profiles is between 0.6 K at the ground to 1.5 K at 2 km above sea level (Fig. 3.3).

See end of chapter 3.4 for data management.

3.3 Shadowband radiometer observations for cloud and aerosol property retrieval

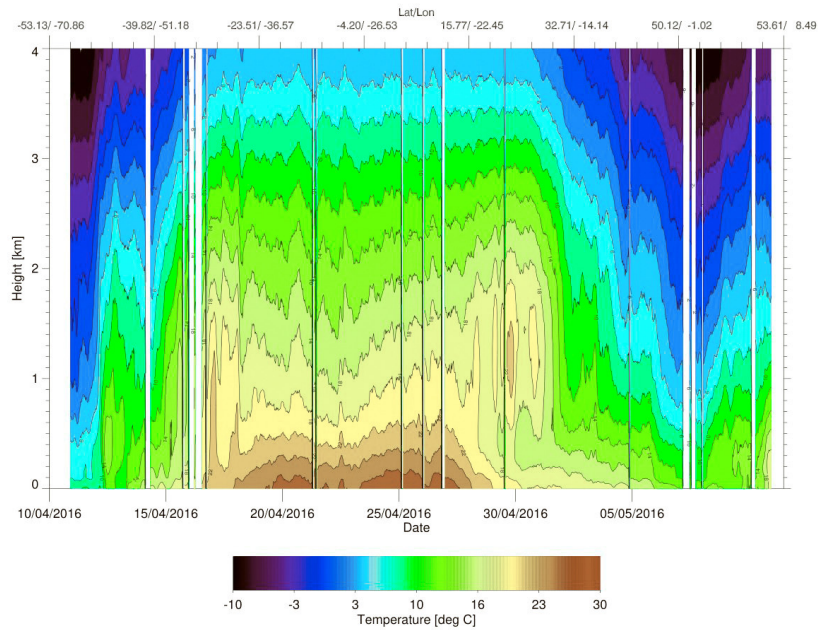


Fig. 3.2: Temperature cross-section during PS98 derived from microwave radiometer observations using elevation scans

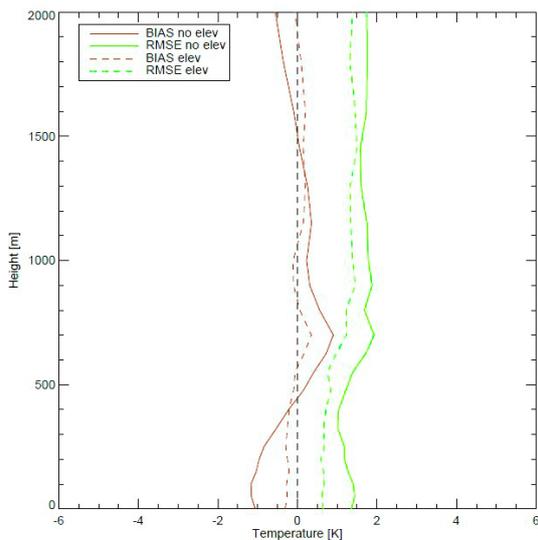


Fig. 3.3: Bias and root mean square error (RMSE) between microwave radiometer observations and simultaneous radiosondes during PS98. Solid lines represent zenith looking observations only, dashed lines use also elevation scans.

3.3 Shadowband radiometer observations for cloud and aerosol property retrieval

Tobias Kuchler

Tropos Leipzig

Objectives

Another measuring instrument taking part on the OCEANET-project is the ground-based ultraviolet and visible shadowband radiometer GUVis-3511 designed by Biospherical Instruments Inc. The radiometer is equipped with a GPS-sensor and a motor which rotates a shadowband subassembly over the radiometer. This shadowband is a bowed band that blocks

a small part of the sky during one sweep. It sweeps every minute over the sensor. One sweep takes roughly 40 s. This sweeping occurs for solar zenith angles below 85°. This rotating shadowband allows the application of the radiometers on the ship. Other components are an instrument control unit and a PC with the data acquisition software “μlogger”. The radiometer measures solar irradiances with a resolution of 15 Hz at 18 narrowband channels from 305 nm to 1,640 nm. The datasets are then corrected to compensate the ship motion. These datasets are used to calculate global, direct and diffuse irradiances and the aerosol optical depth (AOD). The calculation of AOD is only possible if there is no cloud in front of the sun disk.

Work at sea

The shadowband radiometer was installed on an iron rod at the front right corner on the top of the OCEANET container at 10 April. On the same rod an all-sky imager was mounted. A weather-resistant shielded cable connected the radiometer to the control unit. The control unit was connected to a PC. The measurement started at the same day and stopped in the morning of 11 May. During the measurements an all-sky camera took pictures every 15 seconds.

The software recording the data caused some trouble. During the measurements the software shut down several times per day and thus it had then to be restarted which caused some data gaps.

Preliminary (expected) results

Fig. 3.4 shows the Ångström exponent in dependence of atmospheric optical depth (AOD). It is related to the particle size and thus aerosol classes can be defined. The classes can be identified by the colored boxes in Fig. 3.4. It can be well seen that aerosols that occurred during the cruise originated mainly from ocean or deserts. Marine aerosols were observed on 22 April in the subtropics (blue dots). Desert dust was present during the second half of this cruise due to the proximity of the Saharan desert. From the shadowband data there were also cases with biomass burning or continental aerosols (green dots). Another instrument (MICROTOPS II, section 4 of this report) also analyzed continental aerosols for these cases. when the origin of the air masses was over the continent. At other days no or weak continental influence can be seen.

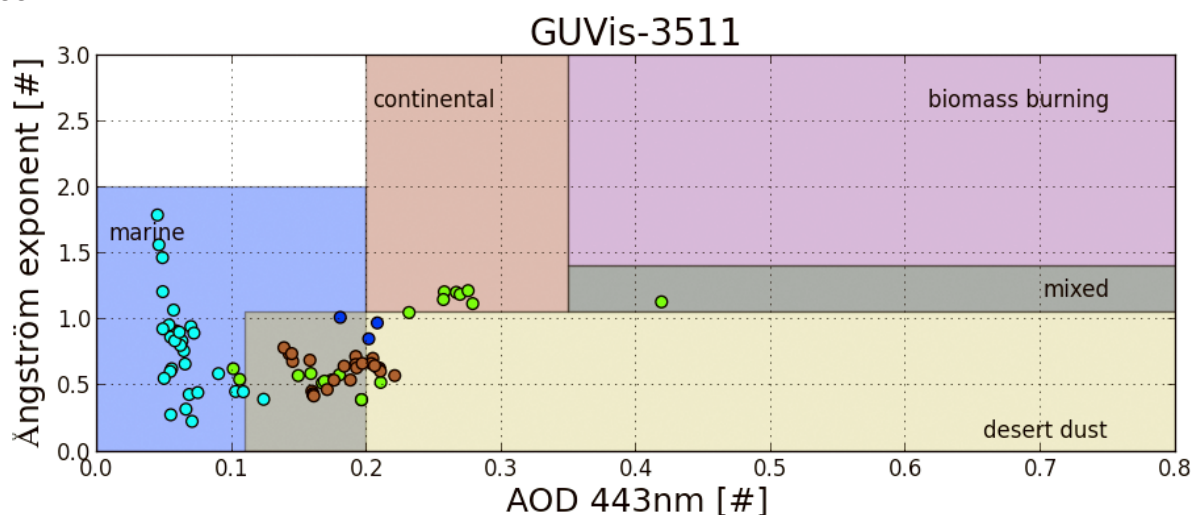


Fig. 3.4: Ångström exponent as a function of aerosol optical depth at 443 nm. The colored rectangles show the ranges of several aerosol types. The color of the dots indicates the observed range of days.

3.4 Infrared camera measurements for temperature profiling

Johannes Stapf TROPOS Leipzig

Objective and work at sea

To test the capabilities of deriving temperature profiles from infrared camera measurements during clear sky conditions, brightness temperature profiles were recorded. Therefore, a Jenoptik VARIOSCAN 3021 ST thermal infrared camera (Fig. 3.5a) was used with a sensor integration range between 8 and 14 μm . Usually this kind of camera systems are used in building or engineering thermography, however the high temporal and spatial resolution offers certain advantages also in atmospheric applications.

Preliminary results

Due to a field of view of $20^\circ \times 30^\circ$ (240 x 360 pixel) single images have to be stitched, resulting in a panorama covering zenith angles from 0 to 90 degree. An example of such a brightness temperature profile can be seen in Fig. 3.5 b, which was taken on 29 April 2016. Using radiative transfer simulations, a temperature profile could be estimated (Fig. 3.5c). In direct comparison to the radiosonde the derived temperature profile for the scene of Fig. 3.5b shows a smoothing of the prevailing temperature inversion, but roughly reproduces the actual profile recorded by the radiosonde.

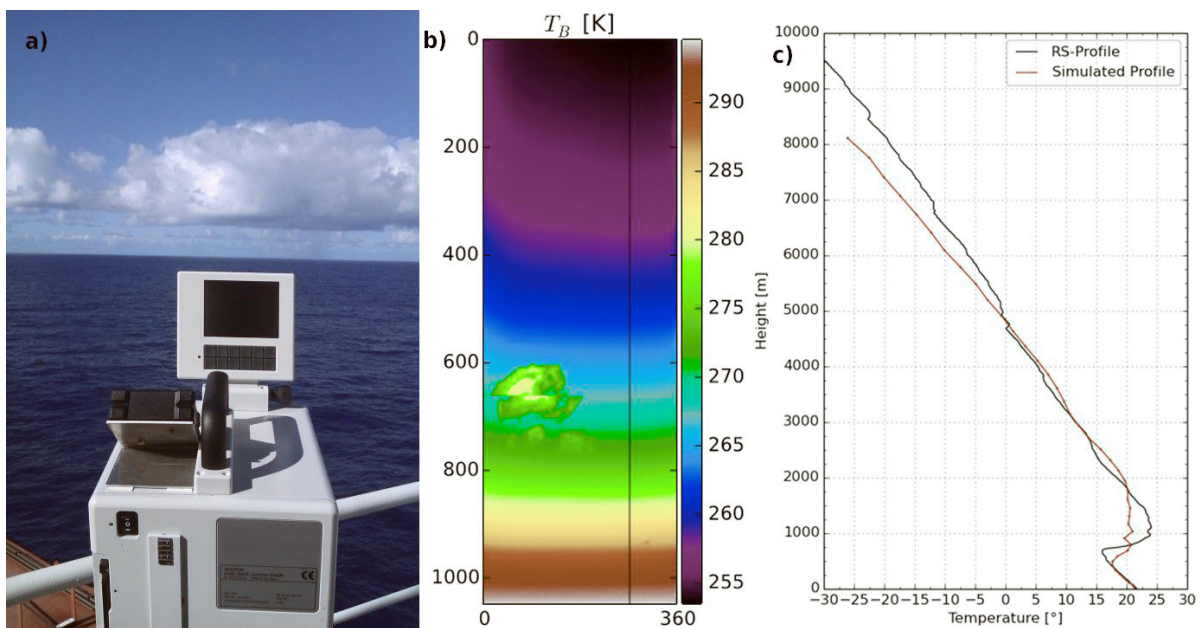


Fig. 3.5 a) VARIOSCAN 3021 ST during PS98. (Photo: Johannes Stapf) b) Stitched brightness temperature profile taken on 29 April 2016. c) Temperature profile derived from IR-Camera measurement (red) in comparison to the radiosonde (black) on 29th April 2016.

Data management

All remote-sensing data processing was carried out at TROPOS and the Leipzig Institute for Meteorology (LIM). The quality checked data will be made available through the PANGAEA database after the cruise.

4. DOCUMENTING AEROSOL AND CLOUD PARAMETERS ACROSS DIFFERENT OCEANIC CLIMATE REGIONS

Stephan Bakan, Christiane Duscha

MPI-M

AWI_PS98_00

Introduction

Transfer cruises of *Polarstern* between northern Germany and the southern Atlantic Ocean provide welcome and valuable opportunities for the collection of climatological data along almost meridional cross-sectional tracks and for the test and evaluation of new observational instruments and methods. The Max-Planck-Institute for Meteorology (MPI-M, Hamburg, Germany) used the PS98 cruise for activities in both fields.

The main contribution consisted of handheld Microtops sun photometer measurements in several spectral bands, resulting in quantitative estimates of aerosol optical depth, particle size, and atmospheric water vapor column. In addition, the group tested a combined system of thermal infrared and visible wide angle cameras for day and night control of cloudiness. Furthermore, special attention was given to the performance of a high quality precipitation disdrometer deployed at *Polarstern* by the OceanRAIN project of the University of Hamburg since a few years.

Work at sea

4.1 Aerosol extinction measurements

General

The main contribution of the MPI-M consisted of aerosol extinction measurements in several visible and near infrared spectral bands with a handheld Microtops II sun photometer (Fig. 4.1). The instrument records direct solar radiation through parallel mounted small telescopes with filters at 380, 440, 675, 870, and 936 μm . Another small telescope projects the sun on a target disk for correct alignment before recording the measurement. After corrections for molecular and gaseous extinction these measurements allow to derive the aerosol optical depth, indicators of aerosol particle size, and the atmospheric water vapor column.

These measurements are part of the maritime component of AERONET, a NASA coordinated worldwide network of ground-based remote sensing activities (Smirnov et al., 2009). Dr. Stefan Kinne from the Max-Planck-Institute for Meteorology in Hamburg (Germany) organized since long such aerosol measurements on German research vehicles and recruited also this time a crew (Fig. 4.2) for these observations during the PS98 cruise.



Fig. 4.1: Microtops II handheld multichannel sun photometer (right) and attached GPS receiver (left)

4.1 Aerosol extinction measurements

After initial difficulties due to adverse weather conditions, it was possible to submit almost daily valid observations to the NASA GSFC data center (Fig. 4.3).

Aerosol optical depth measurements

Comparison with results from another successful cruise during April/May 2008 shows general similarities as well as remarkable differences in details (Fig. 4.4). In many locations north of about 10°S the aerosol optical depth tends to be substantially smaller this time.

This is especially obvious for the aerosol load off the African coast, where the stronger reduction with wavelength hints also at substantially smaller particles this time. Together with back trajectory information from the German Weather Service (DWD), this indicates that the aerosol load off the Northwest African coast was this time less determined by Saharan mineral dust but much rather by sub-Saharan biogenic smog particles.



Fig. 4.2: Christiane Duscha und Stephan Bakan at work

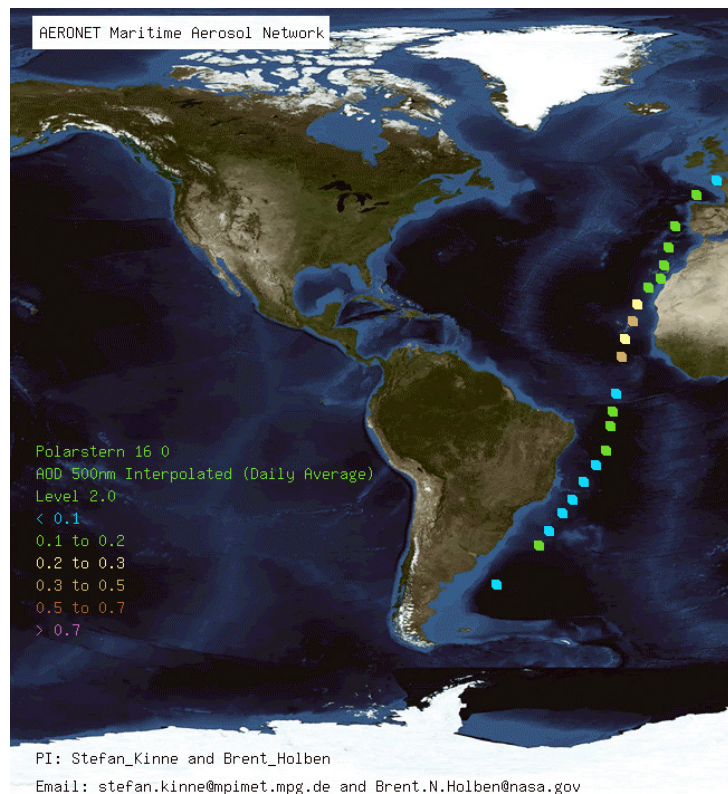


Fig. 4.3: Location (dots) and value (color) of daily average aerosol optical depth measurements at 500nm during the first half of the PS98 cruise

(Adjusted from: aeronet.gsfc.nasa.gov/new_web/cruises_new/Polarstern_16_0.html)

Another interesting episode with comparatively small optical depth and larger particles was recorded during the passage of the Bay of Biscay north of 40°N. While approaching the northern coast of Spain a small low pressure center approached rapidly from the northwest Atlantic, slowed down upon its arrival and proceeded slowly northeastward during the following two days. During that time *Polarstern* remained more or less constantly in the northern part of

this fresh and clean marine air mass with small optical depth and rather large (presumably sea salt) aerosol particles.

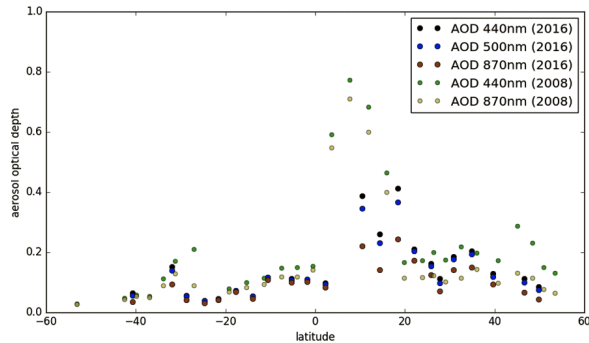


Fig. 4.4: PS98 observations of aerosol optical depth in comparison with results during a similar cruise in April/May 2008

Water vapor column measurements

Surface based sun photometer measurements in the near infrared spectral range have been used since long for the remote determination of the total atmospheric water vapor column (e.g.: Thome et al., 1992). Within the oceanic component of AERONET, the Microtops sun photometer measurements in the 940 nm band are regularly used for columnar water vapor retrievals (with algorithms based on Michalsky et al., 1995, and Schmid et al., 1996).

There are obviously not too many evaluation studies of the quality of AERONET columnar water vapor records over the ocean available. As the meteorology crew on *Polarstern* launches regular daily radiosondes at 12 UTC plus additional soundings at special request of the scientific crew, these data have been used for comparison of results. From the vertical temperature $T(z)$ and relative humidity $RH(z)$ profiles the vertical water vapor column in cm was calculated and compared to our AERONET data.

Fig 4.5 shows the result for 21 comparable cases, indicating a systematic underestimation of the water vapor column by 0.24 cm with a standard deviation of 0.22 cm. Similar results are found (but not shown here) in another preliminary comparison with water vapor column estimates from the HATPRO microwave profiler on board, that was operated by our colleagues from the University of Leipzig. These preliminary indications of a systematic bias of AERONET water vapor column estimates during the PS98 cruise have to be carefully and systematically checked with more data.

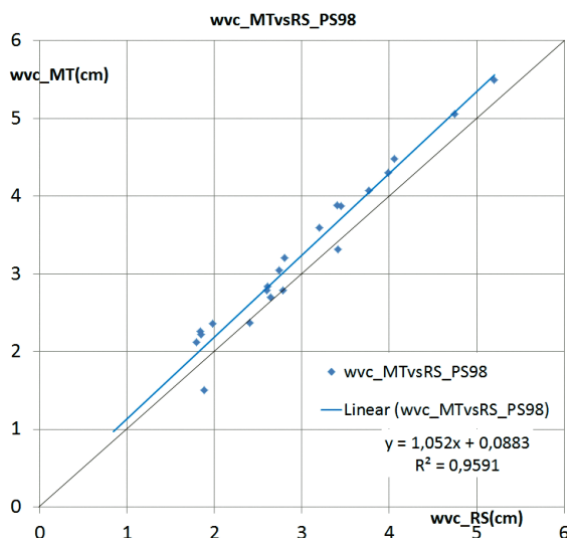


Fig. 4.5: Atmospheric water vapor column (in cm) estimated from the Microtops measurements (wvc_MT) in comparison with control values from coinciding radiosoundings (wvc_RS)

4.2 Cloud observations

As a second activity, a combined system of thermal infrared and visible wide angle cameras for day and night control of cloudiness was tested, and an available automatic cloudiness extraction software was further adjusted and optimized for the present task.

Instrument Setup

During earlier ship cruises a vertically pointing high quality thermal IR camera (VarioCam, Infratec) was deployed repeatedly by the MPI-M group for cloud documentation. To protect the camera from adverse environmental disturbances (as e.g. sea spray), it was mounted into a simple compact housing. This was however often unable to dissipate enough heat (produced by the camera) for proper camera operation, especially under warm tropical conditions.

Therefore, this time the camera was integrated into the top plate of an insulating box with thermoelectric cooling inside for better control of the operation temperature (see Fig. 4.6). Besides the camera electronics, this box contained the data collecting PC with the IRBIS camera software. To protect the IR-camera also from direct solar incidence, at least during small sun elevation angles, a narrow annulus was mounted around the camera optics. This annulus functioned also as basis for a protection lid during daytime with higher sun elevation. The upper rim of this annulus was somewhat slanted and supported a thin IR transmitting plastic foil to protect the camera optics from rain. The camera optics provided an opening angle of about 60°.

In addition, a small camera for the visible spectral range (Mobotix Flexmount) with a somewhat larger opening angle was mounted next to the IR-camera. This camera was intended to provide daytime cloudiness monitoring and control cloud images during overlap periods with the IR camera. The latter could help with the evaluation of IR derived cloudiness values.

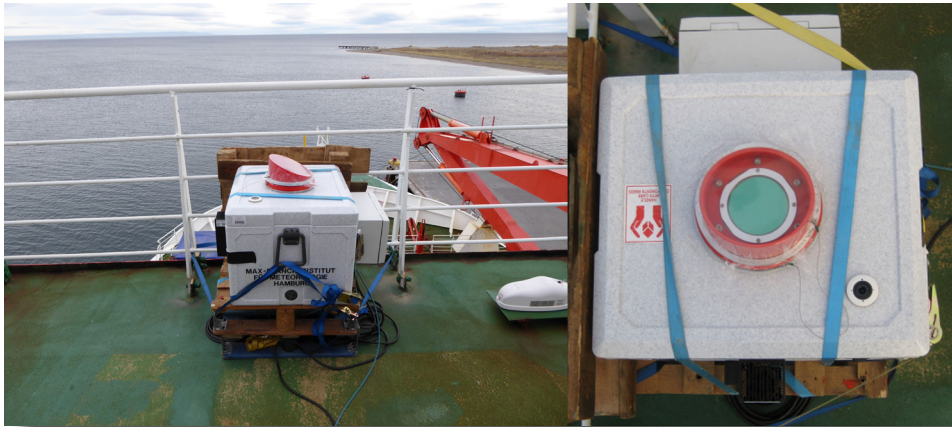


Fig. 4.6: Camera deployment during PS98

During the PS98 cruise, the camera box was placed at and strapped to the railing on the bow side of the monkey island above the bridge of *Polarstern*. Opposite to the railing, the camera's view was partly covered by the crow's nest and, in the case of the VIS camera, also by some antenna on both other sides. Still this place was the least disturbed from sea spray, ship exhaust, and passenger traffic, found on the ship.

Measurements

The cameras were operated almost daily between 10 April and 10 May. During camera operation, every 10s images from the VIS and the thermal IR camera were saved to the local computer in the camera box, amounting to a total of almost half a million stored images.

The RGB images from the VIS camera were usually recorded 24 hours a day and saved as uncalibrated JPG files. In application for cloud detection, especially the colour difference between the red and blue channels (R-B) should be a useful quantity. The application of such a procedure is however useless in direct sunlight conditions, where significant parts of the picture are saturated by the direct solar incidence and the bright forward scattering lobe around the sun's position. During night time there is usually not enough sky brightness for useful cloud imaging. During moonlit nights, clouds were however recognizable on the recorded VIS images. In cloudless night conditions without moonlight, stars could be clearly recognized. There was however not enough time available during the cruise to explore the potential of the VIS images for cloud detection or cloudiness determination in any detail.

The single valued pixel images of the thermal IR camera were saved as calibrated IRB brightness temperature files (proprietary image format). For further use in cloudiness analysis, these IRB pixel values were later converted to ASCII and also to JPG format for simple visual inspection. As the detector array of the IR camera is very sensitive to direct solar irradiation, IR imaging was limited to the night time interval between dusk and dawn with the sun being below horizon or at low elevations.

VIS as well as thermal IR images during and sometime after precipitation events are useless for cloud analysis due to shading and distortions by droplets accumulating and remaining for some time on the camera aperture.

Fig. 4.7 shows a typical clear sky brightness temperature image of the IR camera, taken on the evening of 24 April under subtropical conditions. The colour coding is defined by the colour wedge at the right hand side of the image, spanning a temperature range between -4 and $+23^{\circ}\text{C}$. Most of the actual image represents the thermally cool cloud free sky by the dark blue area. On the right-hand side however, some elements of the crow's nest stick out by their much higher brightness temperature indicated with reddish colors. And at both upper edges the camera looks at the shading annulus, which also radiates at fairly high temperatures of around 23°C , which is only about 5 degrees less than the environmental temperature. These environmental image elements are excluded from the later analysis by applying a simple rectangular image mask.

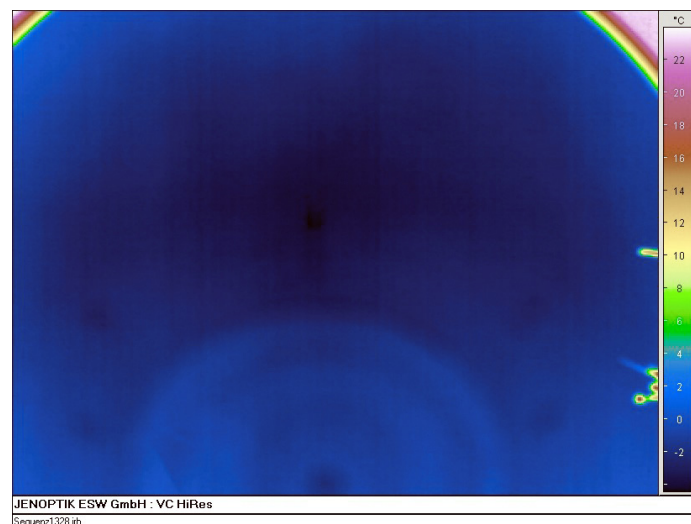


Fig. 4.7: Thermal IR image of a clear sky scene on 24. April, 21:58:57 UTC

The brightness temperature of the clear sky part varies by about 6°C across the image, increasing with distance from the coldest point roughly in the middle. This is most probably due to the thermal emission of the covering plastic foil, which is highly but not completely

4.2 Cloud observations

transparent in the thermal infrared. In addition, another half circular disturbance with somewhat higher brightness temperature is visible in the lower third of the field of view. This is most probably due to heating of the plastic foil from the relatively warm interior of the insulating box through the camera optics lenses. These disturbances have to be accounted for in order to expect reliable results for cloud analysis.

An example of broken subtropical boundary layer cumulus clouds can be seen in Fig. 4.8. Here the brightness temperatures cover a range between -1°C in a clear sky patch near the image center and 24°C at the annulus, which is only about 4°C below environmental temperature. Optically thick clouds exhibit brightness temperatures of about 6 degrees below environmental, indicating cloud bases of below 1000 meters above ocean surface. The edges of these clouds show smaller brightness temperatures due to either higher levels of cloud filaments or reduced optical thickness. Detached from the few centers of very low level clouds a few smaller cloud filaments at a spectrum of ever smaller brightness temperatures are visible. These may be higher level clouds or partially transparent low clouds or a mixture of both. On the right side faint structures appear at brightness temperatures of about 4 degrees above the coolest central area, suggesting the existence of another layer of higher level clouds. The earlier mentioned half-circular emission structure of the cover foil in the lower image part may well disturb the proper detection of such higher level clouds. But for the determination of low level clouds this emission structure can obviously be well ignored in comparison to other uncertainties. Finally, it should be noted that the point-like warm feature near the center in Fig. 4.8 is the thermal image of the moon that can clearly be seen moving across the field of view throughout the night.

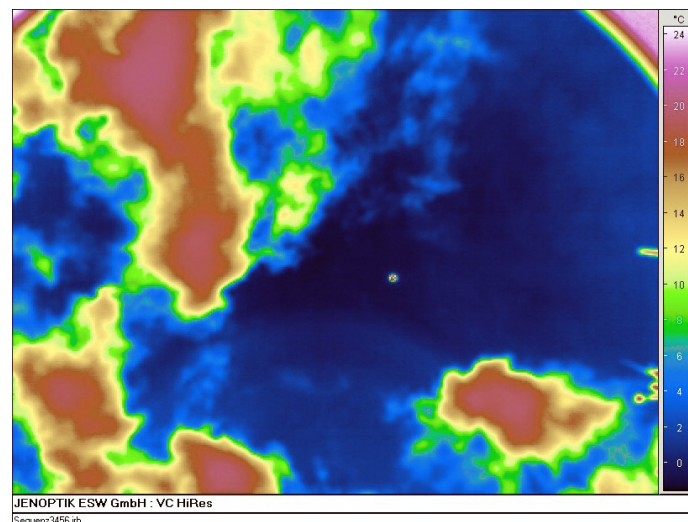


Fig. 4.8: Thermal IR image (24 April, 03:53:37 UTC) of a broken cloud scene with low and high level clouds and the moon near the center

Thermal IR cloud detection and cloudiness determination

The available thermal IR camera was already successfully operated during earlier *Polarstern* cruises and the images have been used to detect clouds and to derive time series of cloud fraction (vve.g.: Fuchs, 2013; Schulz, 2016). In the course of our analysis refinement, two different methods to evaluate the cloud fraction were developed on the basis of the software implemented by Nils Fuchs.

The first and simpler method uses a minimum cloud brightness temperature threshold to define low level clouds. All pixels with smaller brightness temperatures than the threshold are consequently recognized as clear sky or higher level clouds. In contrast to earlier practice, the threshold was not defined as a fixed temperature value but it was chosen relative to the

sea surface temperature (SST). Brightness temperatures between 0 and 12°C below SST are assumed to correspond to cloud heights below about 2 km, the climatologically defined top height for boundary layer clouds. Analyzed results with this method look plausible and promising. It should however be mentioned here that due to the threshold algorithm for low clouds, their cloudiness may be calculated too small due to the smaller brightness temperatures of mixed pixels with thin cloud filaments near the cloud edges. For later routine application of such a method the sensitivity of the threshold value should be evaluated from situations with known height information from e.g. ceilometer measurements.

Total cloudiness, including mid and high level clouds cannot reliably be detected by this method. The clear sky brightness temperature distribution is too variable throughout the image (cf. Fig. 4.7) for simply defining a fixed threshold. Therefore, an average clear sky threshold brightness temperature image was created from phases of consecutive clear sky cases. Fig. 4.9 shows an example for the early evening of 23 April together with the brightness temperature frequency distribution. The standard deviation at each pixel turned out to be typically well below 1°C. This average image was subtracted from each individual image in the analyzed time interval. Positive pixel values in the resulting difference images correspond to cloudy conditions while pixel values around or below zero characterize cloud free conditions. The fraction of such defined cloudy pixels represents the total cloudiness in the image.

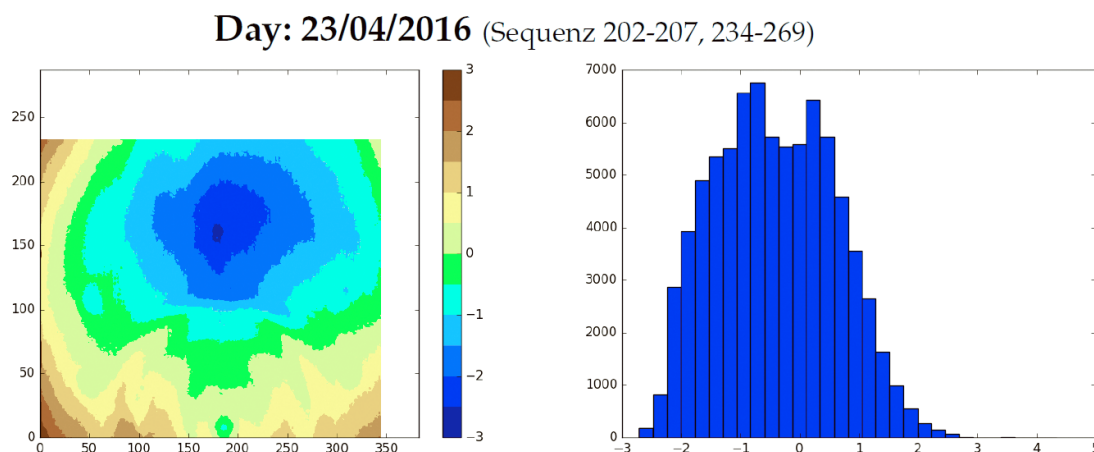


Fig. 4.9: Average thermal IR clear sky image (left, temperature difference from masked image mean) and brightness temperature frequency distribution (right) for 42 clear sky image sequences around 18 UTC on 23 April

The value of this procedure is shown for the image case in Fig. 4.10. This image contains obviously only higher level clouds with brightness temperatures of more than 20°C below the environmental 28°C. The brightness temperature histogram of this image after applying the mentioned mask is shown on the left hand side of Fig. 4.11. This diagram is stretched across about 10 degrees with no clear separation between background and cloudy pixels. But after subtracting the averaged clear sky image (Fig. 4.9) the resulting right hand frequency distribution in Fig. 4.11 exhibits a fairly clear separation of colder clear sky and warmer higher level clouds.

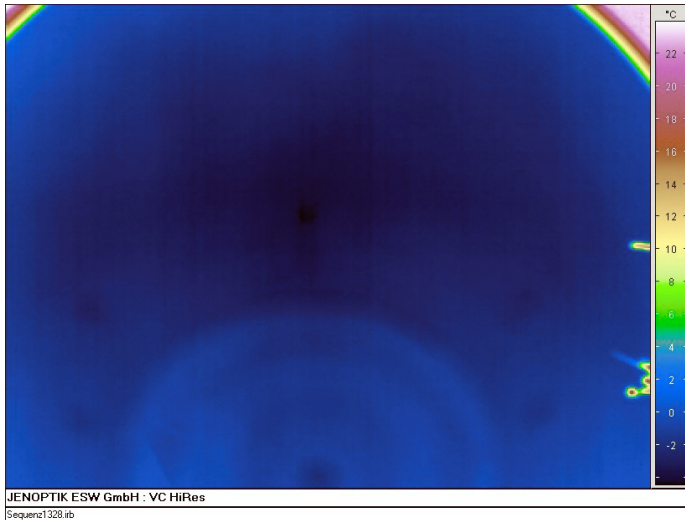


Fig. 4.10: Thermal IR image (23 April, 23:37:27UT) of a scene with some clear sky and high level clouds

To account for some scatter in the procedure only pixels with differences larger than 1°C are counted as cloudy, otherwise as clear sky. The resulting fraction of cloudy pixels determines the total cloud fraction of the image, which is usually larger than the one calculated with the first method for boundary layer clouds only.

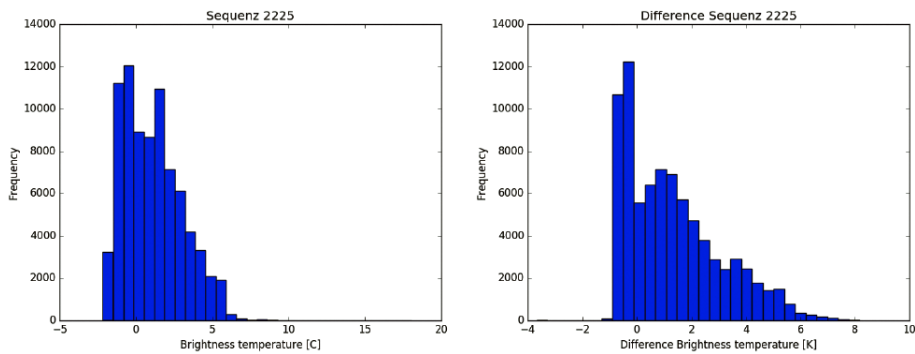


Fig. 4.11: Brightness temperature frequency distribution of the thermal IR image from Fig. 4.10 before (left) and after (right) the subtraction of the average clear sky background image

To demonstrate the implemented methods, the time period between 24 April, 18 UTC, and 25 April, 11 UTC, is chosen from the PS98 cruise. During that night the ship was travelling a distance of about 300 km from $5^{\circ}9'S/26^{\circ}40'W$ to $2^{\circ}27'S/26^{\circ}16'W$ with time periods of clear sky, broken clouds and overcast sky. Both methods to derive boundary layer and total cloudiness were applied to almost 6,000 recorded image frames. For better overview the individual results were averaged over periods of 10 minutes. SST and environmental temperature during that night were around $28,5^{\circ}\text{C}$ and $28,0^{\circ}\text{C}$, respectively.

Fig. 4.12 shows that the resulting total cloud fraction is always larger than the low cloud fraction as should be expected. For comparison also the 10-minute averaged cloud ceiling time series from the onboard laser ceilometer is displayed. In phases of longer lasting low level cloudiness (as e.g. during a precipitating phase around 3 UTC) the ceilometer exhibits fairly small ceiling heights of below 1 km. During that phase both low level and total cloudiness reached 100 percent coverage. Occasionally only high level clouds are detected as e.g. in a phase before 21 UTC, which is also reflected in the large ceiling height. Towards the end of the night *Polarstern* crossed another patch of mostly higher level clouds for quite some time. Accordingly, the ceilometer record suggests midlevel clouds at a few thousand meters height.

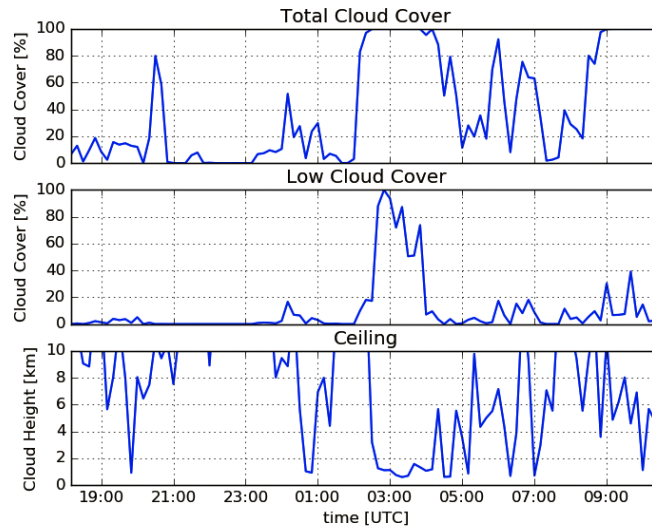


Fig. 4.12: 10 minute averages of total (top) and low level (middle) cloud fraction as derived from IR sky images and of cloud ceiling (bottom) from the onboard ceilometer during the night 24/25 April 2016

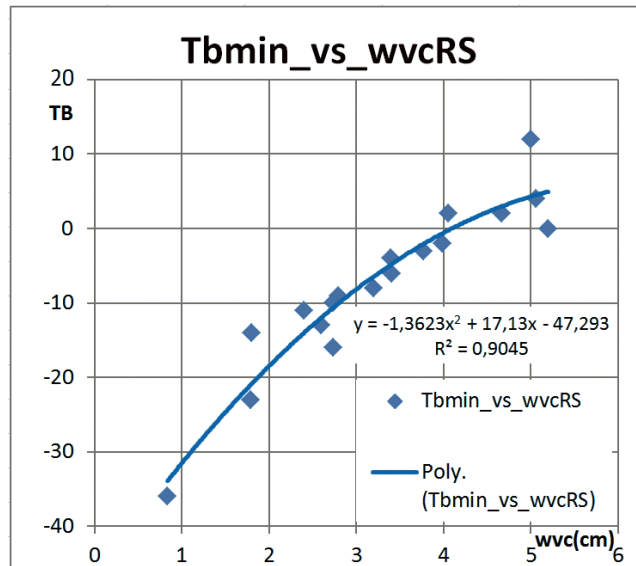


Fig. 4.13: Minimum thermal IR image brightness temperature vs. water vapor column

Relation between thermal IR clear sky images and water vapor column

Combining the water vapor column estimates from Ch. 2.3 with the thermal IR images of clear sky scenes results in an interesting proportionality with some application potential. To explore this proportionality, the minimum infrared brightness temperatures of clear sky images are plotted in Fig. 4.13 vs. the total water vapor column from a nearby radiosounding. Within increasing water vapor column, the clear sky minimum brightness temperature increases as expected from physical principles. For larger values the brightness temperature tends obviously towards saturation. A quadratic function fits the relation between the two quantities fairly well.

Such a relation suggests to set up a catalogue of background clear sky temperature images for different water vapor columns. This could be useful to derive total cloudiness for many situations without completely clear sky episodes in near temporal distance. To increase the data volume, the water vapor column determination from the AERONET data set or the available HATPRO microwave measurements could conveniently be used.

4.3 Other activities

During PS98 special attention was given to the performance of a precipitation disdrometer deployed to the *Polarstern* by the OceanRAIN project of the University of Hamburg (Klepp, 2015). These data are supposed to serve as long-term ground reference for satellite based precipitation estimates. By documenting weather conditions during precipitation phases carefully the data base for the evaluation of the instrument performance has been notably improved.

Preliminary results

In total the PS98 cruise is considered to have been very successful by our group. We collected more than 2000 high quality sun photometer measurements for the AERONET project and contributed substantially to the ever larger collection of aerosol information over the global oceans. We started to evaluate the AERONET water vapor column data derived from our observations. As they turned out to be larger than comparison data from other sources, more effort is recommended to clarify this issue.

We were able to test successfully the operation of a newly constructed combination of thermal IR and VIS cameras in a cooled box environment. We made new steps towards improving the determination of total and low level cloud fractions from surface based thermal IR imaging. Results from one observation period of 18 hours shows mostly results that seem to correspond satisfactorily with parallel ship ceilometer measurements. This calls for an extension of the analysis and an additional validation effort of the retrieval results with available ceilometer and satellite data.

Data management

The quality-checked data are available to the public via the NASA GSFC data center under the web address „aeronet.gsfc.nasa.gov/new_web/cruises_new/Polarstern_16_0.html“.

Acknowledgement

The authors of this report are grateful for that once in a lifetime scientific and personal experience to sail the whole Atlantic Ocean from Punta Arenas to Bremerhaven. We would especially like to thank the ship's crew as well as our scientific colleagues for their help and understanding in all respects of such a cruise and for the inspiring and enjoyable time together on the marvelous *Polarstern*.

References

- Fuchs N (2013) Wolkenklassifikation anhand multispektraler bodengebundener Fernerkundungssysteme. Bachelor Thesis, Universität Hamburg, 35p.
- Klepp C (2015) The Oceanic Shipboard Precipitation Measurement Network for Surface Validation – OceanRAIN. Atmos. Res., Special issue of the International Precipitation Working Group (IPWG), 163, 74-90, doi: 10.1016/j.atmosres.2014.12.014.
- Michalski JJ, Liljegren JC and Harrison LC (1995) A comparison of Sun photometer derivations of total column water vapor and ozone to standard measures of same at the Southern Great Plains Atmospheric Radiation Measurement site. J. Geophys. Res., 100, D12, 25995-26003.
- Schmid B, Thome KJ, Demoulin P, Peter R, Mätzler C, Sekler J (1996) Comparison of modeled and empirical approaches for retrieving columnar water vapor from solar transmittance measurements in the 0.94- μm region. J. Geophys. Res., 101, D5, 9345-9358.
- Schulz H (2016) Personal communication.
- Smirnov A, Holben BN, Slutsker I, Giles DM, McClain CR, Eck TF, Sakerin SM, Macke A, Croot P, Zibordi G, Quinn PK, Sciare J, Kinne S, Harvey M, Smyth TJ, Piketh S, Zielinski T, Proshutinsky A, Goes JI, Nelson NB, Larouche P, Radionov VF, Goloub P, Krishna Moorthy K, Matarrese R, Robertson EJ, Jourdin F (2009) Maritime Aerosol Network as a component of Aerosol Robotic Network, J. Geophys. Res., 114, D06204, doi:10.1029/2008JD011257.
- Thome KJ, Herman BM, Reagan JA (1992) Determination of precipitable water from solar transmission. J. Appl. Meteorol., 31, 157-165.

5. ANIMAL TRANSPORT FOR STUDIES ON TEMPERATURE AND HYPOXIA TOLERANCE OF VARIOUS LIFE STAGES OF LITHODID CRABS

Fredy Véliz Moraleda¹, Marcel Machnik¹, Corina Peter¹, Rodrigo Lorenzo²
not on board: Daniela Storch¹, Astrid Wittmann¹

¹AWI
²CADIC-CONICET

AWI_PS98_00

Objectives and scientific programme

The aim of this project was to transport living king crabs (egg-carrying females and males, *Lithodes santolla* and *Paralomis granulosa*) from Punta Arenas to Bremerhaven. The animals will be used in experiments of the DFG Project STO 857/2-1 "Climate driven Antarctic invasion? Physiological impacts of temperature and hypoxia on life stages of reptant decapod crustaceans and implications for distribution shifts". The main objectives were:

Purchase of animals in Punta Arenas

- Installation of aquaria systems on board of *Polarstern*
- Transport of animals from the aquarium "Laredo" of the Universidad de Magallanes of Punta Arenas to the aquarium of the AWI, Bremerhaven with *Polarstern*
- Maintaining animals during the cruise from Punta Arenas to Bremerhaven
- Control of water parameters in the systems



Work at sea

Fig. 5.1: A recirculation system in a biolab container on board of Polarstern (left photo). Each system contained of 5 tanks which were connected via U tubes. Each tank was equipped with air bubble stones to ensure air saturation of the sea water. Five to six animals were located per tank depending on the size of the animals (right photo).

Recirculating systems

Three re-circulating systems were installed in three temperature-controlled Biolaboratory containers located on deck F of *Polarstern*. Each system consisted of 5 big tanks filled with well aerated seawater (Fig. 5.1). The animals were kept in these systems for the entire cruise. Moulting *L. santolla* males were separated during the time of moulting.

Animals and state

King crabs were purchased from local fishermen in Punta Arenas and maintained in the aquarium "Laredo" of the Universidad de Magallanes of Punta Arenas until *Polarstern* arrived. On 10 April 2016, *L. santolla* (n = 28 females, n = 41 males) and *P. granulosa* (n = 11 females) were transferred from the Aquarium "Laredo" in Punta Arenas to the Biolab containers on board of *Polarstern* by means of a fisher boot because *Polarstern* was lying in the roads. Upon arrival on *Polarstern*, *L. santolla* were marked, measured and egg stages were documented. Furthermore, the moulting state was assessed for the males of *L. santolla*. All animals were not fed during the cruise and dead individuals were removed.

Water parameters

Water parameters (nitrite, ammonium, salinity, temperature and oxygen) were controlled on a daily basis. Nitrite and ammonium samples were taken in the mornings and measured photometrical. Temperature and salinity were measured in the mornings, before and after the seawater was exchanged in the systems. Oxygen and temperature were continuously monitored with two IKS aquastar systems in the recirculating system 1 and 2. Both IKS were equipped with an oxygen and a temperature sensor.

Seawater was exchanged in each of the three systems once or twice every day. Therefore, seawater was pumped from the sea surface into a special cooling tank on board (capacity: 1,100 l) whilst *Polarstern* was moving. Temperature and salinity of the incoming seawater was adjusted to the desired temperature and salinity in the cooling tank. Subsequently the sea water was pumped from the cooling tank in the system 1,2 or 3, respectively. Salinity was adjusted by adding tap water provided by *Polarstern*. The water temperature corresponded to an un-stressful low temperature for the crabs and were adjusted to maintain the metabolism of the animals low.

Preliminary results

Recirculating systems

All systems were installed successfully while *Polarstern* was lying in the roads in Punta Arenas and were running during the cruise without any major problems. At the beginning the U-tubes to connect the tanks within one system were leaky and had to be sealed. On day 12 of the cruise, one U-tube of system 1 emptied completely and five females were exposed to air for some time.

System 1 contained all females of *L. santolla*, with 5-6 animals per tank. *P. granulosa* females were maintained in one tank of system 2, whereas the remaining 4 tanks of system 2 were occupied by males of *L. santolla*. In system 3 only *L. santolla* males were kept.

Animals and state

Females had mean carapace width and length of 11.7 ± 0.4 cm and 11.2 ± 0.4 cm (n = 28), respectively. All females carried eggs without eye spots. The colour of the eggs ranged between light orange and dark red, indicating an early to intermediate egg stage (Table 5.1). Males were only slightly bigger compared to the females with carapace width and length of 12.1 ± 1.1 cm

5. Studies on Temperature and Hypoxia Tolerance of various Life Stages of lithodid Crabs

and 11.2 ± 1.0 cm (n = 37), respectively. Thirteen males were identified as pre-moult stages (Table 5.2) and most of those moulted. In total 14 males moulted during the cruise. Ovigerous females of *P. granulosa* (n = 11) were not measured on board of *Polarstern*.

Tab. 5.1: Size and egg stage of *L. santolla* females measured upon arrival on *Polarstern* on 10 April 2016. All animals were labelled with consecutive numbers, carapace width and length were measured and egg stage documented. Definition of amount of eggs: many: eggs reach coxa, medium: eggs are regularly distributed under the abdomen. The colour of the eggs indicates the egg stage and were distinguished from early to advanced developmental stages: light orange, orange, medium orange, dark orange to red and dark red. None of the females carried eggs with eye spots. * indicates females that died during the cruise.

Females			Egg stage		
Number	Width [cm]	Length [cm]	Colour of eggs	Eye spot	Amount of eggs
1	12	10.9	medium orange	none	medium
2	11.4	11.3	dark orange	none	medium
3	11.6	11.5	dark rot	none	medium +
4	12.3	11.2	dark red	none	medium
5	11.5	11.2	dark orange	none	medium -
6*	10.7	10.2	dark orange	none	medium
7*	11.8	11.2	dark orange	none	many
8	11.5	11.5	dark orange	none	medium -
9	12.1	11.7	dark orange	none	medium
10	12.4	12	dark orange	none	medium +
11	11.5	10.8	orange	none	medium -
12	11.8	11.1	dark orange	none	medium +
13	11.95	11.5	dark red	none	many
14	12.1	12	orange	none	medium
15	11.5	10.9	dark orange	none	many
16	11.2	11.15	dark red	none	many
17*	11.9	11.1	dark orange	none	medium +
18	11.7	11	orange	none	medium
19	11.1	10.9	orange	none	medium
20	11.6	11	dark red	none	medium +
21	12.2	11.5	dark orange	none	medium +
22	11.5	11	light orange	none	medium +
23	11.8	10.9	dark orange	none	many
24*	11.6	11.2	red	none	medium +
25	11.9	11.4	dark orange	none	many
26	11.5	11.2	dark orange	None	medium +
27	11.2	10.6	orange	None	medium +
28	11.8	11.2	dark red	None	medium

Mortality

Overall mortality of *L. santolla* was 30 % whereas more males (n = 17) than females (n = 4) died during the cruise (Fig. 5.2 A). Only one *P. granulosa* female died on day 17 on board. Females of *L. santolla* and *P. granulosa* were in good condition. Two females of *L. santolla* died 2 days after their recirculation system failed (on day 12). There were no apparent reasons for the death of the other two females.

Highest mortality of *L. santolla* males (n = 12) occurred within the first 12 days and was partly explained by injuries such as crushed carapace or swollen abdomen (n = 6) and autotomized legs (n = 1) due to the fishing procedure. The other males that died at the beginning were in their pre-moult or moult phase (n = 5) (Table 5.3). Males were more vulnerable to the fishing and handling stress because during this time of the year males are naturally in their moulting phase and the carapace is not as robust as in the inter-moult phase. After the initial high mortality one further male with an autotomized leg died; three males died in the pre-moult phase or during the moulting process; and one healthy male died on day 28 of the cruise (Fig. 1A).

At the end of the cruise 24 females and 24 males of *L. santolla* (Fig. 5.2 B) and 10 females of *P. granulosa* arrived in good condition in Bremerhaven and were successfully transported to the AWI aquarium.

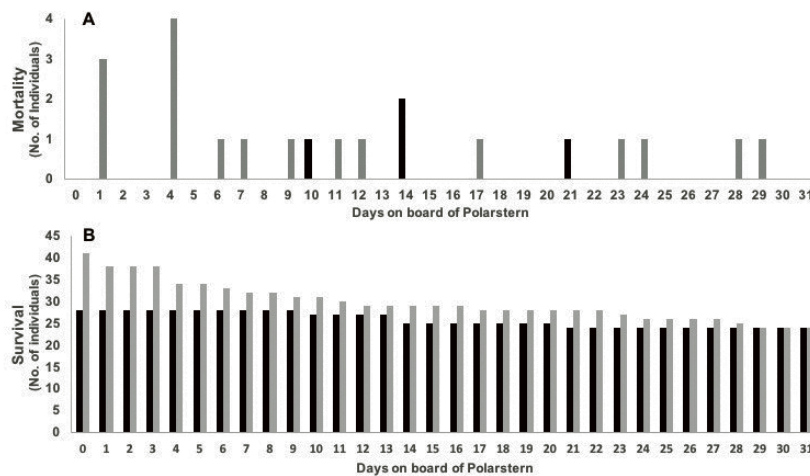


Fig. 5.2: Mortality (A) and resulting survival (B) of *L. santolla* during the Polarstern cruise PS 98. In total 17 males and 4 females died resulting in 24 females and 24 males that survived the cruise and were transported to the aquarium of the AWI in Bremerhaven. (females: black bars, males: grey bars)

Tab. 5.2: Size and state of *L. santolla* males measured upon arrival on *Polarstern* on the 10. April 2016. All males were labelled with consecutive numbers, carapace width and length were measured and the state of each individual was documented. * indicates males that died during the cruise.

Males			
Number	Width [cm]	Length [cm]	State
1	11.9	10.8	early pre-moult
2*	12.6	11.4	late pre-moult
3	11.1	9.9	fine
4	9.6	9.5	epiphytes on carapace
5	12.9	11.6	healthy
6	13.2	12.4	autotomized leg
7	10.7	10	fine

5. Studies on Temperature and Hypoxia Tolerance of various Life Stages of lithodid Crabs

Males			
Number	Width [cm]	Length [cm]	State
8	11.2	10.4	epiphytes on carapace
9	10.7	10.2	healthy
10	11.5	10.5	healthy
11	11.8	10.7	fine
12	14.8	13.45	healthy
13*	10.8	10.1	autotomized leg
14	13.5	12.6	healthy
15*	11.2	10.6	swollen abdomen
16*	13.2	12.2	slightly broken carapace
17	10.8	9.7	healthy
18*	11.9	11	healthy
19*	11.2	10.5	autotomized leg
20	Not measured		dead
21	12	11	slightly broken carapace
22*	13.8	12.3	epiphytes on carapace, broken carapace
23	11.5	10.5	late pre-moult
24	10.9	10.2	early pre-moult
25	13.9	13.2	early pre-moult
26*	13.2	11.8	soft abdomen
27*	12.4	11.5	early pre-moult
28*	13.3	13	early pre-moult
29	11.9	11.4	(moulted recently)
30	11.6	10.6	early pre-moult
31	12.3	11.7	early pre-moult
32	13.6	12.9	early pre-moult
34green	11.8	11.2	early pre-moult
34red*	11.4	10.8	early pre-moult
35	12	10.8	epiphytes on carapace
36*	13.2	12.6	late pre-moult
37*	Not measured		dead
38	11.1	11	abdomen diseased
39	11.8	10.85	crushed carapace, swollen abdomen
40*	Not measured		dead
41*	Not measured		moulted on 10/4

Tab. 5.3. State and number of *L. santolla* males that died or survived during the cruise

State of male	Dead	Survivors
Crushed carapace or swollen abdomen	6	0
Abdomen diseased	0	1
Autotomized leg	2	1
Healthy	1	10
Early pre-moult	2	2
Late pre-moult	2	0
Moulted during cruise	4	10

Water parameters

Daily morning measurements of nitrite, ammonium, temperature and salinity in the three systems are represented in Fig. 5.3. Nitrite values are considered as optimal or acceptable for the maintenance of animals in the ranges between 0.00 – 0.10 mg/l and <0.2 mg/l, respectively. Nitrite concentration in the systems ranged from 0.02 mg/l to maximal 0.12 mg/l with mean values of 0.03 ± 0.01 mg/l in system 1; 0.05 ± 0.03 mg/l in system 2 and 0.06 ± 0.03 mg/l in system 3 (Fig. 5.3 A).

Ammonium increased to unfavourable values (> 0.4 mg/l) in all systems during the first 5 days and decreased to acceptable concentrations (< 0.4 mg/l) until the end of the cruise (Fig. 5.3 B).

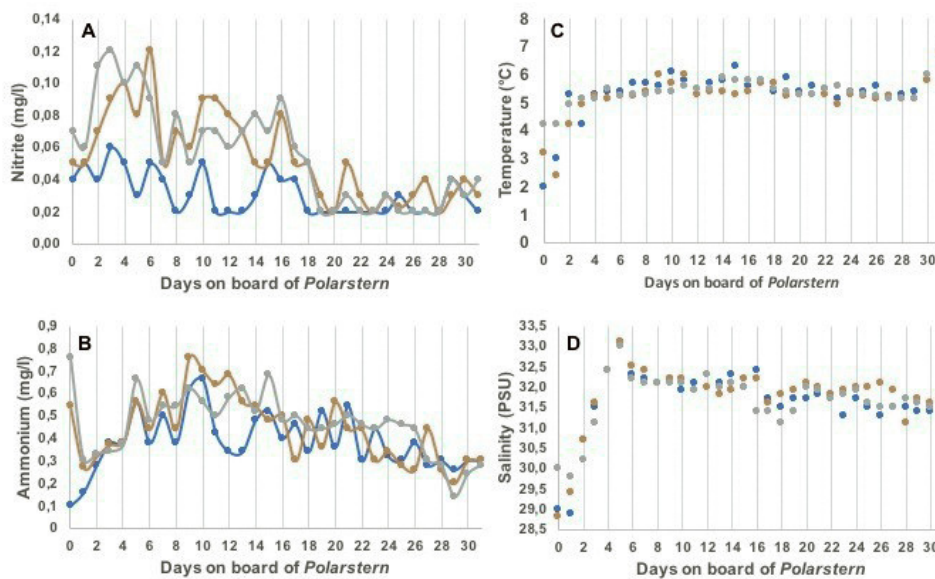


Fig. 5.3: Daily morning measurements of nitrite (A), ammonium (B), temperature (C) and salinity (D). System 1: blue lines and dots, system 2: orange lines and dots, system 3: grey lines and dots. Each dot represents one measurement.

Ammonium peaked during days with dead animals in the system. The initial increase of ammonium can be explained by the increase of temperature and salinity during the first 5 days until temperature and salinity values stabilized to 5-6°C and around 32 PSU, respectively

5. Studies on Temperature and Hypoxia Tolerance of various Life Stages of lithodid Crabs

(Fig. 5.3 C & D). Ammonium values could not be decreased to acceptable values at lower latitudes with high sea surface temperatures due to the limiting number of water exchanges per day (maximal 4 per day). The limiting factor for the number of water exchanges per day was the cooling capacity of the water tank. At lower latitudes with temperatures above 20°C the cooling tank took longer to adjust the temperature and thus, could be refilled only 4 times a day. Close to the equator incoming seawater reached a temperature of up to 28.9°C and a salinity of 37.59 PSU (Fig. 5.4 A & B). After passing the equator sea surface temperature started to decrease and the cooling tank was refilled up to six times a day and water exchanges in the systems were increased accordingly.

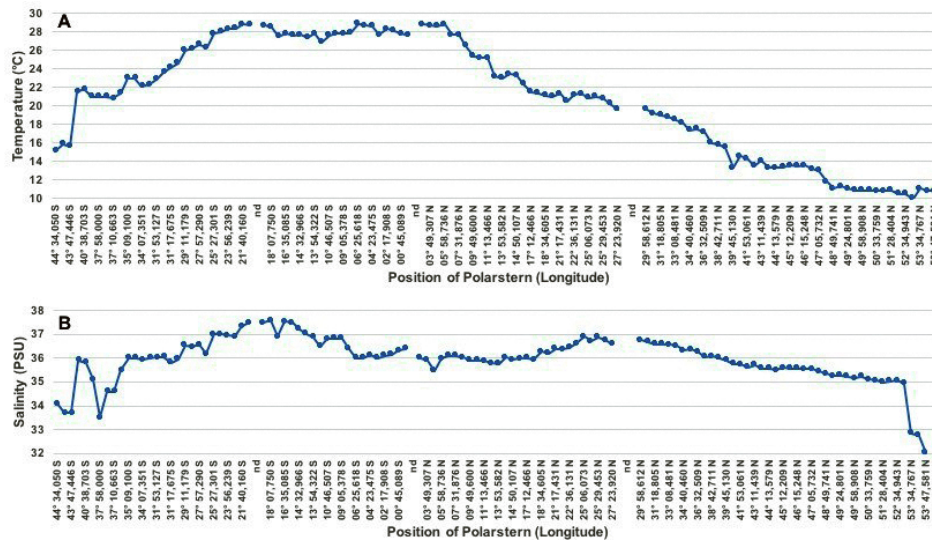


Fig. 5.4: Temperature and salinity of the sea surface during the cruise PS 98 from Punta Arenas to Bremerhaven. Each data point represents the position of Polarstern where the cooling tank was refilled. Depending on the temperature and salinity of the incoming seawater, water exchanges varied between 3 and 6 times a day.

Just before the arrival in Bremerhaven, the temperature in the systems was slowly increased to around 7°C to acclimate the animals to the warmer seawater temperature prevailing the AWI aquarium.

Continuous measurements of temperature and oxygen by means of the IKS systems are depicted in Fig. 5.5 A & B for system 1 and in Fig. 5.6 A & B for system 2. Oxygen and temperature decreased steeply during each water exchange because sensors were exposed to air. Continuous and daily morning measurements of temperature show the same results (Figs. 5.5 A, 5.6 A & 5.3 C). Oxygen saturation of the seawater was in both systems optimal and were always > 90 %.

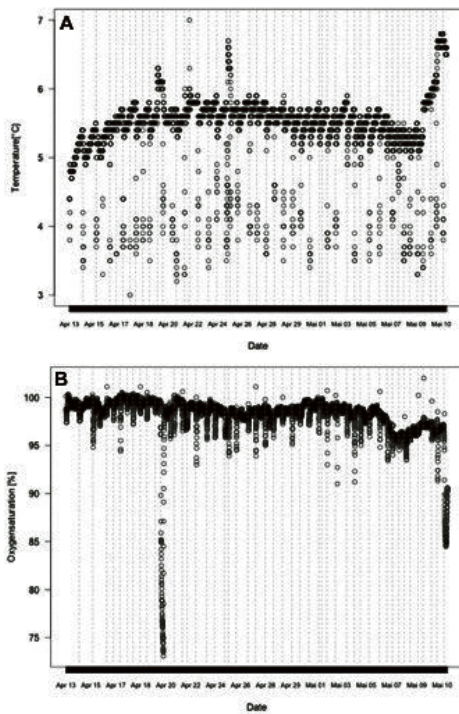


Fig. 5.5: Continuous recording of temperature (A) and oxygen expressed as % air saturation (B) in the recirculation system 1.

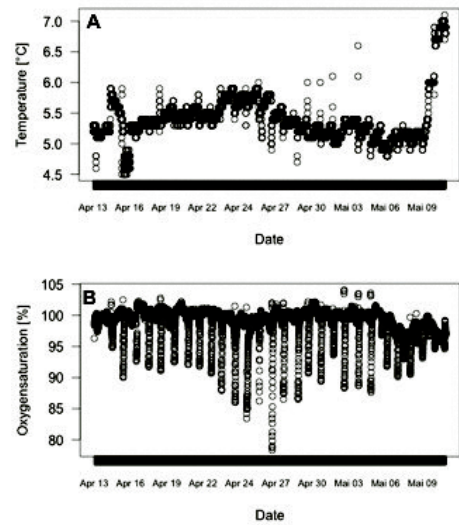


Fig. 5.6: Continuous recording of temperature (A) and oxygen expressed as % air saturation (B) in the recirculation system 2.

Data management

Data taken during lab experiments back in Bremerhaven will be made available after validation through the PANGAEA database. Results will be included in the Master thesis of Corina Peter, the PhD thesis of Rodrigo Lorenzo and will be published in international Peer-reviewed journals.

6. ECHOSOUNDING TRAINING CRUISE (POLMAR-TRAIN 2016)

Gerhard Kuhn¹, Frank Niessen¹, Boris Dorschel¹,
Catalina Gebhardt¹, Simon Dreutter², Claudia
Sprengel¹, Claudia Hanfland¹ (not on board)
Master Students and doctoral candidates:
Dilip Adhikari², Saeid Bagheri³, Tim Daskevic³,
Yuri Dvornikov⁴, Johanna Fall⁵, Sebastian
Höpker³, Amr Ibrahim², Islam Ibrahim², Male
Köster³, Margaret Lindeman¹, Juan Manuel Lirio⁶,
Tamara Manograsso⁶, Henning Marinkovic³,
Melissa Mengert³, Florian Schmid¹, Jan
Schürman³, Lara Steinbrink³, Jiawei Tang³

¹AWI
²HafenCity Uni Hamburg
³Uni Bremen
⁴AWI Potsdam
⁵Uni Bergen
⁶IAA

AWI_PS98_00

Objectives

POLMAR-TRAIN 2016 is a student training course that was jointly run by the AWI-based Helmholtz Graduate School for Polar and Marine Research (POLMAR) and the University of Bremen. The purpose was to provide master students and doctoral candidates from the field of geosciences with a hands-on training in operating the hull-mounted echosounding systems of *Polarstern* (multibeam echosounder Atlas Hydrosweep DS3 and sediment echosounder Parasound P70). Parallel to the practical training, the aim was to promote peer-learning by combining master students (beginners and advanced stage) and doctoral candidates / scientists in this course.

POLMAR-TRAIN is part of the programme “Master of Sciences Marine Geosciences” at the University of Bremen as well as of the scientific programme of POLMAR. Both programmes involve ship-based field-work for students and doctoral candidates. The training was carried out by five lecturers affiliated with both the University of Bremen and AWI.

Work at sea

Educational Aspects

Thirteen master students from the University of Bremen and HafenCity University Hamburg and seven doctoral candidates/ scientists from AWI, the Argentine Antarctic Institute (Inst. Antártico Argentino), and the Institute of Marine Research in Bergen participated in the training. Study topics of the students includes geology, geophysics, marine biology, sea-ice physics, and oceanography.

The course started with a theoretical introduction into the physics of echosounding, followed by a general introduction into the operating systems. Afterwards, students started going on watches (generally 4 hours each) in pairs of two for each system. Watches were organised in a way that in each case beginners and more experienced students and PhD students / scientists were jointly responsible for one system. This approach aimed at learning amongst peers and proved to be successful. Master students benefited from the research experience of the postgraduates, could discuss possible topics for their master thesis and clarify their motivation for the next career step including the option of taking up doctoral studies.

In groups of four, participants discussed regional examples (e.g. Lomonosov Ridge, Baffin Bay) in order to apply and deepen their knowledge. They learned to interpret submarine geomorphological structures from bathymetric images, sediment echographs and sediment cores. With regard to multibeam-bathymetric data, participants were introduced to data acquisition, data processing, and visualization with different kind of profiling and GIS mapping software.

All participants gave a 15 min presentation on their Bachelor, Master or PhD project, which provided more examples on the application of echosounding and fostered further discussions.

Technical Aspects

On the way from Las Palmas to Bremerhaven PARASOUND recording was started on 5 May 2016, 08:05 UTC north of Las Palmas (29° 58.6' N, 14° 53.3' W) and ended after the only system crash on 10 May 2016, 10:01 UTC in the Strait of Dover (51° 14.4' N, 1° 51.3' E). Operation stopped after two CM-recoveries and breakdown of telegram transmissions for undetected reasons. The system was switched off thereafter. In total 37.8 GB of data in 5,502 files were recorded. The operational settings of PARASOUND transmissions are summarized in Table 6.1.

Using Software ATLAS PARASTORE PHF and SLF profiles were visualized online. PHF and SLF data were stores in ASD and PS3 formats. In addition, auxiliary data (navigation and PARASOUND settings) were stored in one-minute intervals. Printing of SLF data was performed using a PDF-creator of the operator PC via PNG output formats stored on disc.

Multibeam echosounder data were recorded from 4 May 2016, 08:11 UTC until 10 May 2016, 23:49. In total 66.9 GB of bathymetric data were recorded. The recording was interrupted by several system crashes. Raw data were acquired in the HSDS3 proprietary *.asd format. During post-processing, *.asd files were imported in the hydrographic processing software package CARIS HIPS and SIPS. In CARIS HIPS and SIPS, the data were cleaned for erroneous measurements and spurious soundings. Cleaned data were exported as ASCII xyz and ASCII raster data for visualization and further analyses in ArcGIS.

Tab. 6.1: Settings of ATLAS HYDROMAP CONTROL for operating PARASOUND during PS98

Used Settings	Selected Options	Selected Ranges
Mode of Operation	P-SBP/SBES	PHF, SLF
Frequency	PHF	19 kHz (18.975 kHz)
	SLF	4 kHz (3.987 kHz)
Pulse length	No. of Periods	2
	Length	0.5 ms
Transmission Source Level	Transmission Power	100%
	Transmission Voltage	159 V
Beam Steering	none	
Mode of Transmisson	Single Pulse	Auto according to water depth
	Quasi-Equidistant	Interval 400-1200 ms
Pulse Type	Continuous Wave	
Pulse Shape	Rectangular	
Receiver Band Width	Output Sample Rate (OSR)	6.1 kHz
	Band Width (% of OSR)	66%
Reception Shading	none	

Used Settings	Selected Options	Selected Ranges
System Depth Source	Fix Min/Max Depth Limit	ATLAS PARASOUND PHF
		ATLAS HYDROSWEEP PHF
Water Velocity	C-Mean	Manual 1500 m/s
	C-Keel	System C-keel
Data Recording	PHF	Full Profile, Sediment
	SLF	Full Profile, Sediment

Preliminary results

Educational Aspects

The concept of combining undergraduates and postgraduates in this training proved to be a successful approach. Next to guidance and discussion with the team of lecturers, peer-learning was an important factor for the success of this training concept.

The combination of theoretical background, practical work on the hydroacoustic systems (including troubleshooting), discussion of published data and student presentations was the right combination for a thorough and comprehensive training in echosounding techniques.

Course preparation prior to the cruise was done by the graduate school POLMAR. Participants, lecturers and ship logistics department had one contact point to turn to which greatly improved maintaining the planning phase, coordination on board and the subsequent evaluation phase.

Technical Aspects

During the PARASOUND online operation, two major problems occurred:

(1) When ATLAS HYDROSWEEP PHF was used as System Depth Source for Quasi-Equidistant transmission (Table 6.1), gaps of data were observed at the sea floor and in the upper 200 m of the sediments over a lateral time range of about one minute (at 4,300 m water depth) with a repetition rate of about 30 minutes (Fig. 6.1). These gaps occur when PARASOUND receives wrong depth values from HYDROSWEEP in the moments in which PARASOUND starts to recalculate the pulse rate of transmission. This results in data digitalization of received echoes in the wrong depth interval leading to the data gaps at the sea floor until one of the next reconfigurations is using correct depth (Fig. 6.2). Interestingly, these wrong HYDROSWEEP depth detections are caused by interference with PARASOUND PHF pulses along the center beam (Figs. 6.3 and 6.4). For PARASOUND data acquisition, this problem can be overcome by using ATLAS PARASOUND PHF as System Depth Source (Table 1) as long as sounding conditions allow.

(2) On the operator PC, two SLF echogram windows were active simultaneously during the cruise. One was used to store PS3 data (day-screen color palette). The other was used for printing (online-print color palette). The “print window” often displayed the echograms in the wrong depth interval (Fig. 6.5), while the “data-storage windows” always were correct. In addition, the traces plotted in the wrong depth window appear not to be compensated for ships motion (Fig. 6.5). These errors occurred randomly and had no effect on the actual prints (PNG files) produced out of the echogram windows. The prints were always correct. This error is independent from error **(1)** and could not be overcome.

Throughout the survey, the HSDS 3 had repeated technical problems. Frequent system crashes and subsequent auto-recoveries resulted in data losses. The exchange of the high voltage power module with a spare part increased the system stability.

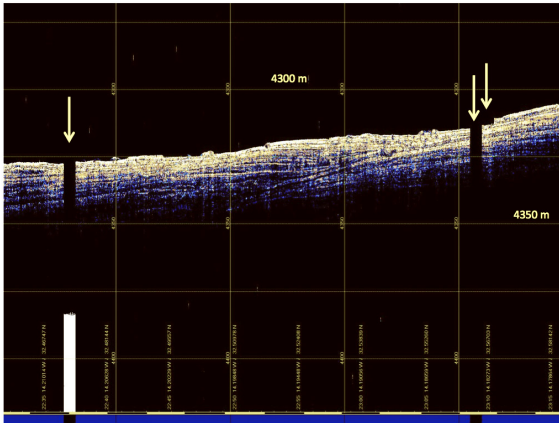


Fig. 6.1: Offline (replay) operation SLF echogram window (200 m vertical scale) with data gaps (indicated by yellow arrows). Data time window from 2016, May 5th, 22:32-23:16 UTC.

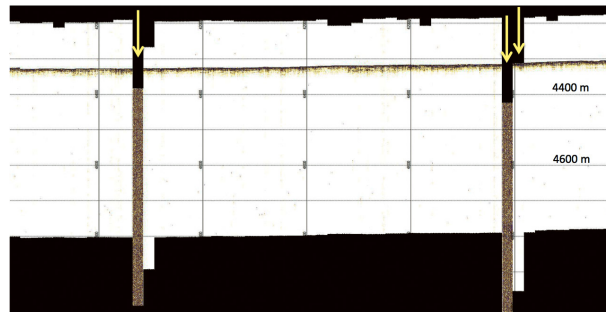


Fig. 6.2: Same as Fig. 6.1 except for 1,000 m vertical scale and different color palette. Clip function is off.

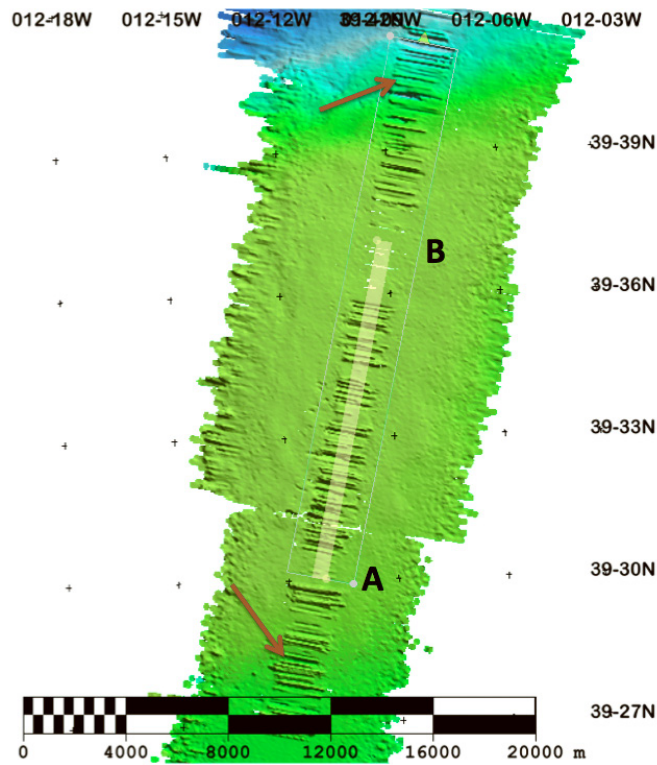


Fig. 6.3: Raw-data example of ATLAS HYDROSWEEEP recorded along track. Note strong interference caused by ATLAS PARASOUND in the center-beam area (indicated by red arrows). Line A to B mark position of bathymetric cross-section displayed in Fig. 6.4. For depth range see Fig. 6.5.

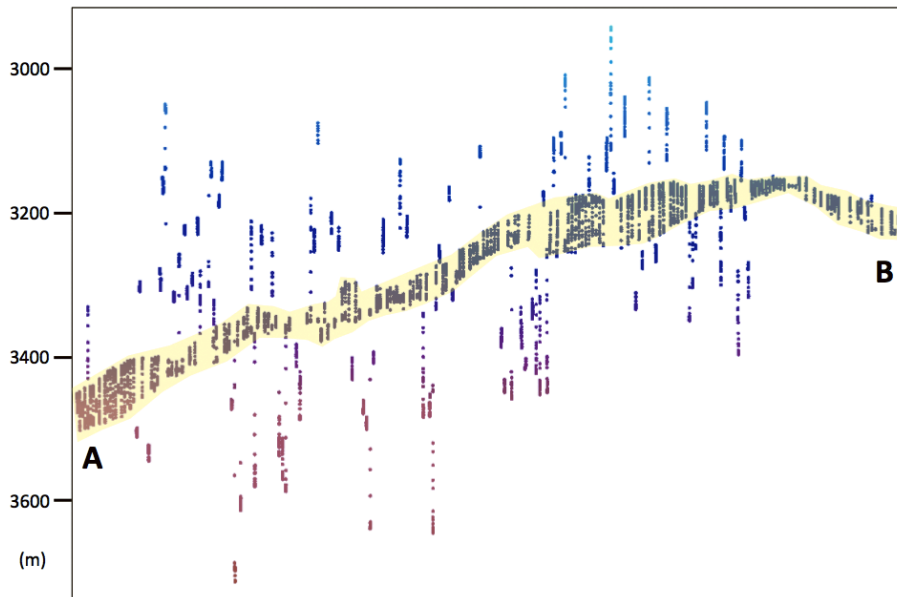


Fig. 6.4: Raw-data example of ATLAS HYDROSWEEP bathymetry recorded along track from the center-beam. Note that data plotted outside the shaded range are artefacts caused by ATLAS PARASOUND. For position of line A to B see map in Fig. 6.3.

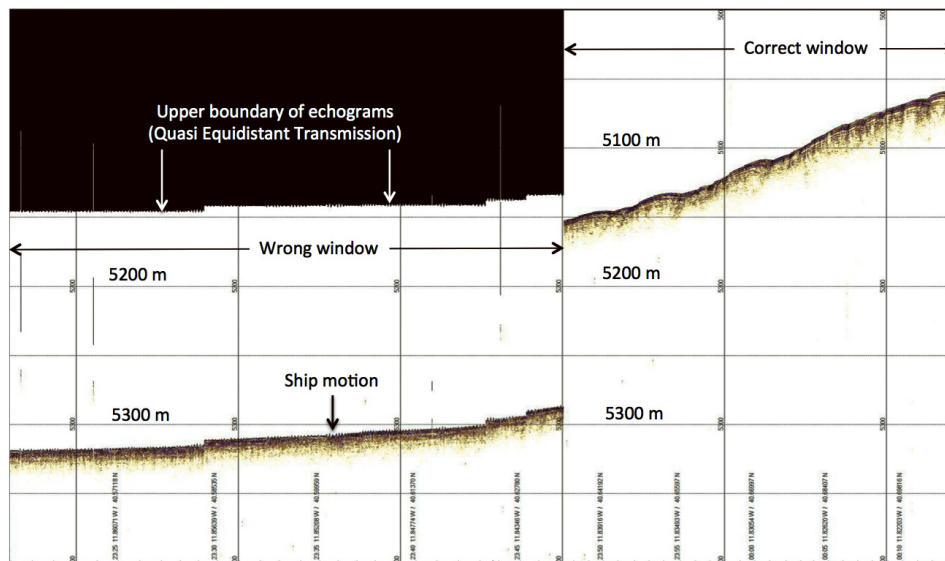


Fig. 6.5: Online operation SLF echogram window (200 m vertical scale) used for printing with echogram examples plotted in the wrong (left) and correct (right) depth range, respectively. Note that the vertical scale remains constant at the visible shift in sea-floor depth by about 140 m. The shift is not operator controlled. Data time window from 6-7 May 2016, 23:20-00:03 UTC.

Data management

Since this was a training course for students, no data was collected for long term storage and publication.

APPENDIX

A.1 PARTICIPATING INSTITUTIONS

A.2 CRUISE PARTICIPANTS

A.3 SHIP'S CREW

A.4 STATION LIST

A.1 TEILNEHMENDE INSTITUTE / PARTICIPATING INSTITUTIONS

	Address
AWI	Alfred-Wegener-Institut Helmholtz-Zentrum für Polar- und Meeresforschung Postfach 120161 27515 Bremerhaven Germany
AWI Potsdam	Alfred-Wegener-Institut Helmholtz-Zentrum für Polar- und Meeresforschung Telegrafenberg A43 14474 Potsdam Germany
CADIC-CONICET	Centro Austral de Investigaciones Bernardo Hoissay 200 V9410CAB Ushuaia, Tierra del Fuego Argentina
Deutscher Wetterdienst	Deutscher Wetterdienst Bernhard-Nocht-Str. 76 20359 Hamburg Germany
HafenCity Uni Hamburg	HafenCity Universität Hamburg Überseeallee 16 20457 Hamburg Germany
IAA	Instituto Antártico Argentino 25 de Mayo 1143, San Martín Provincia de Buenos Aires Argentina

	Address
LIM	Universität Leipzig Leipziger Institut für Meteorologie Stephanstr. 3 04103 Leipzig Germany
TROPOS Leipzig	Leibniz-Institut für Troposphärenforschung e.V. Permoserstraße 15 04318 Leipzig Germany
Uni Bremen	Universität Bremen Bibliothekstraße 1 28359 Bremen Germany
Uni Bergen	University of Bergen P.O.Box 7800 5020 Bergen Norway

A.2 FAHRTTEILNEHMER / CRUISE PARTICIPANTS

Name/ Last name	Vorname/ First name	Institut/ Institute	Beruf/ Profession
Bakan	Stephan	MPI Hamburg	Scientist, meteorology
Bohlmann	Stephanie	TROPOS/Uni Leipzig	MSc student, meteorology
Doktorowski	Tobias	TROPOS/Uni Leipzig	MSc student, meteorology
Duscha	Christiane	MPI Hamburg	MSc student, meteorology
Küchler	Tobias	TROPOS/Uni Leipzig	MSc student, meteorology
Lensch	Norbert	AWI	Technician
Lorenzo	Rodrigo	CADIC-CONICET	PhD student, biology
Machnik	Marcel	AWI Biologie	Technician, biology
Peter	Corina	AWI Biologie	MSc student, biology
Pliet	Johannes	FIELAX GmbH	Technician
Pospichal	Bernhard	Uni Leipzig	Scientist, meteorology
Radenz	Martin	TROPOS/Uni Leipzig	MSc student, meteorology
Rohleder	Christian	Deutscher Wetterdienst	Meteorologist
Sonnabend	Hartmut	Deutscher Wetterdienst	Technician, meteorology
Stapf	Johannes	TROPOS/Uni Leipzig	MSc student, meteorology
Walter	Andreas	AWI Rechenzentrum	Technician
From Las Palmas			
Adhikari	Dilip	HafenCity Uni Hamburg	MSc Student
Bagheri	Saeid	Uni Bremen	MSc Student
Daskevic	Tim	Uni Bremen	MSc Student
Dorschel	Boris	AWI Bremerhaven	Scientist, Lecturer
Dreutter	Simon	HafenCity Uni Hamburg	Scientist, Lecturer
Dvornikov	Yuri	AWI Potsdam	PhD Student
Fall	Johanna	University of Bergen	PhD Student
Gebhardt	Catalina	AWI Bremerhaven	Scientist, Lecturer
Höpker	Sebastian	Uni Bremen	MSc Student
Ibrahim	Amr	HafenCity Uni Hamburg	MSc Student
Ibrahim	Islam	HafenCity Uni Hamburg	MSc Student
Katlein	Christian	AWI Bremerhaven	Postdoc
Köster	Male	Uni Bremen	MSc Student
Kuhn	Gerhard	AWI Bremerhaven	Scientist, Lecturer
Lindeman	Margaret	AWI Bremerhaven	PhD Student
Lirio	Juan Manuel	IAA	PhD Student
Manograsso	Tamara	IAA	PhD Student
Marinkovic	Henning	Uni Bremen	MSc Student

Name/ Last name	Vorname/ First name	Institut/ Institute	Beruf/ Profession
Mengert	Melissa	Uni Bremen	MSc Student
Niessen	Frank	AWI Bremerhaven	Scientist, Lecturer
Schmid	Florian	AWI Bremerhaven	PhD Student
Schürman	Jan	Uni Bremen	MSc Student
Sprengel	Claudia	AWI Bremerhaven	Postdoc
Steinbrink	Lara	Uni Bremen	MSc Student
Tang	Jiawei	Uni Bremen	MSc Student

A.3 SCHIFFSBESATZUNG / SHIP'S CREW

Punta Arenas to Las Palmas

No.	Name	Rank
1.	Schwarze, Stefan	Master
2.	Spielke, Steffen	1. Offc.
3.	Farysch, Bernd	Ch. Eng.
4.	Langhinrichs, Moritz	2. Offc.
5.	Hering, Igor	2. Offc.
6.	Schmidt, Rüdiger	Doctor
7.	Fröb, Martin	R. Offc.
8.	Grafe, Jens	2. Eng.
9.	Krinfeld, Oleksandr	2. Eng.
10.	Holst, Wolfgang	2. Eng.
11.	Redmer, Jens	Elec. Eng.
12.	Christian, Boris	ELO
13.	Hüttebräucker, Olaf	ELO
14.	Lehnert, Lars	ELO
15.	Himmel, Frank	ELO
16.	Loidl, Reiner	Boatsw.
17.	Reise, Lutz	Carpenter
18.	Sandmann, Rainer	A.B.
19.	Scheel, Sebastian	A.B.
20.	Hagemann, Manfred	A.B.
21.	Winkler, Michael	A.B.
22.	Brück, Sebastian	A.B.
23.	Wende, Uwe	A.B.
24.	Bäcker, Andreas	A.B.
25.	Preußner, Jörg	Storek.
26.	Teichert, Uwe	Mot-man
27.	Rhau, Lars-Peter	Mot-man
28.	Lamm, Gerd	Mot-man
29.	Schünemann, Mario	Mot-man
30.	Pinske, Lutz	Mot-man
31.	Redmer, Klaus-Peter	Cook
32.	Silinski, Frank	Cooksmate
33.	Kluge, Wilfried	Cooksmate
34.	Czyborra, Bärbel	1. Stwdess
35.	Wöckener, Martina	Stwdess/N.
36.	Dibenau, Torsten	2. Steward
37.	Silinski, Carmen	2. Stwdess
38.	Arendt, Rene	2. Steward
39.	Grigull, Elke	2. Stwdess

No.	Name	Rank
40.	Sun, Yong Shen	2. Steward
41.	Yu, Kwok Yuen	Laundrym.
42.	Schulz, Fabian	Apprent.
43.	Wittek, Sönke	Apprent.

Las Palmas to Bremerhaven

No.	Name	Rank
1.	Schwarze, Stefan	Master
2.	Spielke, Steffen	1. Offc.
3.	Farysch, Bernd	Ch. Eng.
4.	Langhinrichs, Moritz	2. Offc.
5.	Hering, Igor	2. Offc.
6.	Schmidt, Rüdiger	Doctor
7.	Fröb, Martin	R. Offc.
8.	Grafe, Jens	2. Eng.
9.	Krinfeld, Oleksandr	2. Eng.
10.	Holst, Wolfgang	3. Eng.
11.	Redmer, Jens	Elec. Eng.
12.	Christian, Boris	ELO
13.	Hüttebräucker, Olaf	ELO
14.	Lehnert, Lars	ELO
15.	Himmel, Frank	ELO
16.	Loidl, Reiner	Boatsw.
17.	Reise, Lutz	Carpenter
18.	Sandmann, Rainer	A.B.
19.	Scheel, Sebastian	A.B.
20.	Hagemann, Manfred	A.B.
21.	Winkler, Michael	A.B.
22.	Brück, Sebastian	A.B.
23.	Wende, Uwe	A.B.
24.	Bäcker, Andreas	A.B.
25.	Preußner, Jörg	Storek.
26.	Teichert, Uwe	Mot-man
27.	Rhau, Lars-Peter	Mot-man
28.	Lamm, Gerd	Mot-man
29.	Schünemann, Mario	Mot-man
30.	Pinske, Lutz	Mot-man
31.	Redmer, Klaus-Peter	Cook
32.	Silinski, Frank	Cooksmate

No.	Name	Rank
33.	Kluge, Wilfried	Cooksmate
34.	Czyborra, Bärbel	1. Stwdess
35.	Wöckener, Martina	Stwdess/N.
36.	Dibenau, Torsten	2. Steward
37.	Silinski, Carmen	2. Stwdess
38.	Arendt, Rene	2. Steward
39.	Grigull, Elke	2. Stwdess
40.	Sun, Yong Shen	2. Steward
41.	Yu, Kwok Yuen	Laundrym.
42.	Schulz, Fabian	Apprent.
43.	Wittek, Sönke	Apprent.

A.4 STATIONSLISTE / STATION LIST

Station	Date	Time	Latitude	Longitude	Depth [m]	Gear	Action	Comment
PS98/001-1	2016-04-16	16:32	-34.81517	-44.55017	4796.8	SATP	profile start	
PS98/001-1	2016-04-16	17:39	-34.63667	-44.59917	4760.4	SATP	profile end	
PS98/002-1	2016-04-19	08:45	-25.89100	-38.24800	4192.6	ARGOFL	in the water	ARGO Float7699
PS98/002-1	2016-04-19	08:45	-25.89100	-38.24800	4192.6	ARGOFL	on ground/ max depth	
PS98/003-1	2016-04-20	02:57	-23.05200	-36.24933	4121.8	ARGOFL	in the water	ARGO Float7698
PS98/003-1	2016-04-20	02:57	-23.05200	-36.24933	4121.8	ARGOFL	on ground/ max depth	
PS98/004-1	2016-04-22	08:03	-14.89833	-30.61817	4841.8	ARGOFL	in the water	ARGO Float7697
PS98/004-1	2016-04-22	08:03	-14.89833	-30.61817	4841.8	ARGOFL	on ground/ max depth	
PS98/005-1	2016-04-23	15:00	-10.07983	-27.36767	5588	SATP	profile start	
PS98/006-1	2016-04-23	15:20	-10.02500	-27.37917	5588.3	ARGOFL	in the water	ARGO Float7696
PS98/006-1	2016-04-23	15:20	-10.02500	-27.37917	5588.3	ARGOFL	on ground/ max depth	
PS98/005-1	2016-04-23	16:01	-9.90450	-27.40583	5488.6	SATP	profile end	
PS98/007-1	2016-04-24	19:28	-4.99433	-26.64883	5474.9	ARGOFL	in the water	ARGO Float7695
PS98/007-1	2016-04-24	19:28	-4.99433	-26.64883	5474.9	ARGOFL	on ground/ max depth	
PS98/008-1	2016-04-25	15:10	-1.54617	-26.03583	4687.8	SATP	profile start	
PS98/008-1	2016-04-25	16:12	-1.36617	-26.07367	4894.8	SATP	profile end	
PS98/009-1	2016-04-27	14:46	6.65133	-24.76583	4346.7	SATP	profile start	
PS98/009-1	2016-04-27	15:51	6.83100	-24.80383	4090.2	SATP	profile end	
PS98/010-1	2016-04-29	14:30	14.55617	-23.40117	3869.7	SATP	profile start	
PS98/010-1	2016-04-29	15:32	14.73067	-23.44017	3497.4	SATP	profile end	
PS98/011-1	2016-04-30	03:00	16.24533	-22.15733	2734.8	SATP	profile start	
PS98/011-1	2016-04-30	07:16	16.98300	-21.99417	3441.2	SATP	profile end	

Gear abbreviations	Gear
ARGOFL	Argo float
SATP	Satprofile

Die **Berichte zur Polar- und Meeresforschung** (ISSN 1866-3192) werden beginnend mit dem Band 569 (2008) als Open-Access-Publikation herausgegeben. Ein Verzeichnis aller Bände einschließlich der Druckausgaben (ISSN 1618-3193, Band 377-568, von 2000 bis 2008) sowie der früheren **Berichte zur Polarforschung** (ISSN 0176-5027, Band 1-376, von 1981 bis 2000) befindet sich im electronic Publication Information Center (**ePIC**) des Alfred-Wegener-Instituts, Helmholtz-Zentrum für Polar- und Meeresforschung (AWI); see <http://epic.awi.de>. Durch Auswahl "Reports on Polar- and Marine Research" (via "browse"/"type") wird eine Liste der Publikationen, sortiert nach Bandnummer, innerhalb der absteigenden chronologischen Reihenfolge der Jahrgänge mit Verweis auf das jeweilige pdf-Symbol zum Herunterladen angezeigt.

The **Reports on Polar and Marine Research** (ISSN 1866-3192) are available as open access publications since 2008. A table of all volumes including the printed issues (ISSN 1618-3193, Vol. 377-568, from 2000 until 2008), as well as the earlier **Reports on Polar Research** (ISSN 0176-5027, Vol. 1-376, from 1981 until 2000) is provided by the electronic Publication Information Center (**ePIC**) of the Alfred Wegener Institute, Helmholtz Centre for Polar and Marine Research (AWI); see URL <http://epic.awi.de>. To generate a list of all Reports, use the URL <http://epic.awi.de> and select "browse"/ "type" to browse "Reports on Polar and Marine Research". A chronological list in declining order will be presented, and pdf icons displayed for downloading.

Zuletzt erschienene Ausgaben:

Recently published issues:

720 (2018) The Expedition PS98 of the Research Vessel POLARSTERN to the Atlantic Ocean in 2016, edited by Bernhard Pospichal

719 (2018) The Expeditions PS106/1 and 2 of the Research Vessel POLARSTERN to the Arctic Ocean in 2017, edited by Andreas Macke and Hauke Flores

718 (2018) The Expedition PS111 of the Research Vessel POLARSTERN to the southern Weddell Sea in 2018, edited by Michael Schröder

717 (2018) The Expedition PS107 of the Research Vessel POLARSTERN to the Fram Strait and the AWI-HAUSGARTEN in 2017, edited by Ingo Schewe

716 (2018) Polar Systems under Pressure, 27th International Polar Conference, Rostock, 25 - 29 March 2018, German Society for Polar Research, edited by H. Kassens, D. Damaske, B. Diekmann, D. Fütterer, G. Heinemann, U. Karsten, E.M. Pfeiffer, J. Regnery, M. Scheinert, J. Thiede, R. Tiedemann & D. Wagner

715 (2018) The Expedition PS109 of the Research Vessel POLARSTERN to the Nordic Seas in 2017, edited by Torsten Kanzow

714 (2017) The Expedition SO258/2 of the Research Vessel SONNE to the central Indian Ocean in 2017, edited by Wolfram Geissler

713 (2017) The Expedition PS102 of the Research Vessel POLARSTERN to the Atlantic Ocean in 2016, edited by Karen Wiltshire, Eva-Maria Brodte, Annette Wilson and Peter Lemke

712 (2017) The Expedition PS104 of the Research Vessel POLARSTERN to the Amundsen Sea in 2017, edited by Karsten Gohl

711 (2017) Mid-Range forecasting of the German Waterways streamflow based on hydrologic, atmospheric and oceanic data by Monica Ionita

710 (2017) The Expedition PS103 of the Research Vessel POLARSTERN to the Weddell Sea in 2016/2017, edited by Olaf Boebel



ALFRED-WEGENER-INSTITUT
HELMHOLTZ-ZENTRUM FÜR POLAR-
UND MEERESFORSCHUNG

BREMERHAVEN

Am Handelshafen 12
27570 Bremerhaven
Telefon 0471 4831-0
Telefax 0471 4831-1149
www.awi.de

